Feedback mechanisms controlling Antarctic glacial cycle dynamics simulated with a coupled ice sheet–solid Earth model

Torsten Albrecht [1], Meike Bagge [2,3], and Volker Klemann [2]

[1]Potsdam Institute for Climate Impact Research (PIK), Member of the Leibniz Association, Potsdam, Germany
[2]Helmholtz Centre Potsdam, German Research Centre for Geosciences - GFZ, Potsdam, Germany
[3]now at: Federal Institute for Geosciences and Natural Resources, Hanover, Germany

Correspondence: T. Albrecht (albrecht@pik-potsdam.de)

Abstract. The dynamics of the ice sheets on ~~glacial-interglacial~~ glacial time scales are highly controlled by interactions with the solid Earth, i.e., the glacial isostatic adjustment (GIA). Particularly at marine ice sheets, competing feedback mechanisms govern the migration of the ice sheet's grounding line (GL) and hence the ice sheet stability. ~~In~~ For this study, we ~~run coupled ice sheet–solid~~ developed a coupling scheme and performed a suite of coupled ice sheet–solid Earth simulations over the last two glacial cycles. ~~For the~~ To represent ice sheet dynamics we apply the Parallel Ice Sheet Model PISM and ~~for the load response of~~ to represent the solid Earth ~~we use~~ response we apply the three-dimensional viscoelastic Earth model VILMA, which, in addition to load deformation and rotation changes, considers the gravitationally consistent redistribution of water (the ~~sea level~~ sea-level equation). We decided on an offline coupling between the two model components. By convergence of trajectories of the Antarctic Ice Sheet deglaciation we determine optimal coupling time step and spatial resolution of the GIA model and compare patterns of inferred relative ~~sea level~~ sea-level change since the Last Glacial Maximum with the results from previous studies. With our coupling setup we evaluate the relevance of feedback mechanisms for the glaciation and deglaciation phases in Antarctica considering different 3D Earth structures resulting in a range of load-response time scales. For rather long time scales, in a glacial climate associated with far-field sea level low stand, we find ~~grounding line~~ GL advance up to the edge of the continental shelf mainly in West Antarctica, dominated by a self-amplifying GIA feedback, which we call the 'forebulge feedback'. For the much shorter time scale of deglaciation, dominated by the Marine Ice Sheet Instability, our simulations suggest that the stabilizing ~~GIA~~ sea-level feedback can significantly slow-down ~~grounding line~~ GL retreat in the Ross sector, which is dominated by a very weak Earth structure (i.e. low mantle viscosity and thin lithosphere). This delaying effect prevents a Holocene ~~grounding line~~ GL retreat beyond its present-day ~~location~~position, which is discussed in the scientific community ~~,~~supported by observational evidence at the Siple Coast and by previous model simulations. The ~~described~~ applied coupled framework, PISM-VILMA, allows for defining restart states to run multiple sensitivity simulations from. It can be easily implemented in Earth System Models (ESMs) and provides the tools to gain a better understanding of ice sheet stability on glacial time scales as well as in a warmer future climate.
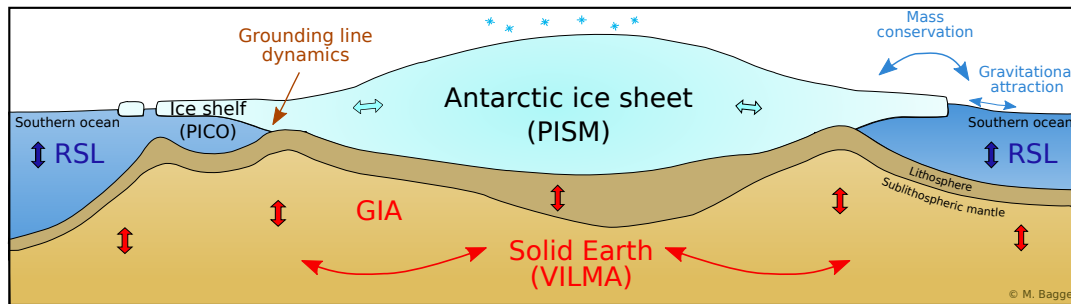
Figure 1. Schematics of coupled PISM Ice Sheet – PICO Ice Shelf – VILMA Solid Earth model components. Bedrock topography, relative sea level (RSL) and ice thickness are exchanged between VILMA and PISM in predefined coupling time steps.

1 Introduction

The observed accelerating retreat of large sectors of the Antarctic Ice Sheet (AIS) raises concerns about future ~~sea level~~
sea-level rise (Seroussi et al., 2020; IPCC, 2021). Self-amplifying, positive feedbacks may trigger the tipping and hence the destabilization and collapse of the marine-based parts of the ice sheet (Pattyn and Morlighem, 2020; Armstrong McKay et al., 2022; Lenton et al., 2023). The Marine Ice Sheet Instability (MISI) is mainly controlled by the bedrock geometry (Fretwell et al., 2013; Morlighem et al., 2020), with retrograde slopes supporting a run-away dynamic feedback mechanism (Weertman, 1974; Mercer, 1978; Thomas and Bentley, 1978; Schoof, 2007), while buttressing forces can have a stabilizing effect for certain ~~ice shelf~~ ice-shelf geometries (Gudmundsson, 2013; Pegler, 2018; Haseloff and Sergienko, 2018; Reese et al., 2018b). The dynamic retreat of ice sheet grounding lines in response to the thinning of ice shelves and the subsequent speed-up of ice streams mainly in West Antarctica have been the dominant drivers of most of the recent mass loss in Antarctica (Rignot et al., 2019; Otosaka et al., 2023), and some studies suggests that MISI may already be underway (Joughin et al., 2014; Rignot et al., 2014; Reed et al., 2023). Depending on the water depth at marine-terminating glacier fronts, the ice sheet retreat may also be amplified by the Marine Ice Cliff Instability (MICI) (Pollard et al., 2015; DeConto and Pollard, 2016; Crawford et al., 2021; Li, 2022).

The solid Earth responds to ice sheet thinning or retreat~~with~~, or more general to loading processes, by viscoelastic deformation, generally known as glacial isostatic adjustment (GIA), see Fig. 1. The strength as well as typical length and time scales of the GIA ~~response~~ depend on the Earth's mantle viscosity and lithosphere thickness (e.g. Peltier, 1974). The consistent redistribution of land ice, ocean water and mantle material induces changes in the Earth'~~'~~s gravity field (with the ~~'geoid' as~~ 'geoid' as an equipotential surface), and therefore alters the sea level globally, which follows the geoid (Farrell and Clark, 1976)~~; a correction, which usually is~~. As a further feedback mechanism, polar motion due to the surface mass redistribution changes the geoid and deforms the solid Earth (Mitrovica et al., 2005). This gravitational-rotational-deformational (GRD) correction is usually considered as being part of ~~GIA.~~ the GIA.

Geodetic and geophysical investigations of crustal uplift in the Amundsen Sea sector in West Antarctica ~~(Barletta et al., 2018; Blank et al~~ (Barletta et al., 2018; Lloyd et al., 2020; Blank et al., 2021) postulate a laterally strongly varying viscoelastic Earth structure

with mantle viscosities orders of magnitude lower than the global average. Hence, a low mantle viscosity implies much faster and, ~~due to a~~ in the likely case of an also thinner lithosphere, a more localised (short-wavelength) response of the solid Earth to ice sheet retreat (van der Wal et al., 2015; Larour et al., 2019; Wan et al., 2022). Furthermore, ~~there is~~ geophysical investigations

50 demand a clear dichotomy in the Earth structure between East and West Antarctica ~~(Behrendt, 1999; Morelli and Danesi, 2004; Accardo et~~ ~~, but~~ (Behrendt, 1999; Morelli and Danesi, 2004; Accardo et al., 2014; Lloyd et al., 2020; Powell et al., 2020). But also within West Antarctica a large degree of heterogeneity exists on length scales of $100\,\text{km}$ (An et al., 2015; Ramirez et al., 2016; Heeszel et al., 2016), with hot spots of enhanced geothermal heat flux (Lough et al., 2013; Dziadek et al., 2021; Bredow et al., 2023).

The relative sea level (RSL), which is the water depth ~~,~~ when positive or more precisely the vertical distance between the
55 geoid and the bottom of the ocean, directly determines the grounding line (GL) position of marine ice sheets via the flotation criterion. A global mean (barystatic) sea level can be calculated from the global RSL change, or by aggregating changes in ice sheet thickness and near-field RSL changes, based on the 'volume above flotation' (Gregory et al., 2019; Goelzer et al., 2020; Adhikari et al., 2020). When ice sheets decay and ~~grounding lines~~ GLs retreat, the ~~GIA-induced viscoelastic bed~~ viscoelastic solid Earth deformation reduces the water depth and hence induces ~~indirectly~~ a stabilizing negative feedback, which is addition-
60 ally supported by near-field sea level lowering in response to reduced gravitational attraction ~~(Gomez et al., 2010, 2012, 2015)~~ ~~.~~ (Gomez et al., 2010, 2012, 2015; Coulon et al., 2021; Han et al., 2021).

As a side effect, the vertical bed displacement induces a bending of the elastic lithosphere and lateral viscous flow of mantle material, which is associated with the migration of a bulge with opposite RSL sign in the vicinity ~~(Adhikari et al., 2014)~~ (Adhikari et al., 2014; Wan et al., 2022). Accordingly, local surface motion and slopes may changes sign during lateral motion
65 of the topographic bulge, which makes it difficult to isolate accelerating or inhibiting effects on the ice flow. During deglacial or interglacial periods, the 'forebulge' subsidence is often associated with a mechanism termed 'ocean syphoning' mainly in view of the northern-hemisphere deglaciation (Mitrovica and Peltier, 1991; Mitrovica and Milne, 2002), which draws water from the far field and thereby contributes a far-field sea-level fall (Powell et al., 2021; Yousefi et al., 2022). The latitudinal extent of the forbulge region strongly depends on the lithosphere thickness. It can be either confined close to the coast and
70 inner continental shelf for a thin lithosphere or reach offshore for thick lithospheres (Stocchi et al., 2013).

In grounded ice sheet regions, where bedrock uplift directly affects the ice sheet's height, the surface climate becomes generally colder and dryer (~~lapse~~ lapse-rate effect), which in turn affects the overall ice dynamics (Van den Berg et al., 2008; Konrad et al., 2014; Zeitz et al., 2022). Potentially, solid-Earth feedbacks can slow down or even halt deglacial retreat, depending on the time scales of the viscoelastic deformation ~~, which depend on~~ controlled by the structure of the solid Earth
75 ~~(Konrad et al., 2015; Larour et al., 2019).~~

(Gomez et al., 2010; Konrad et al., 2015; Larour et al., 2019). In cooling phases with GL advance, i.e. during glaciation, coupled model studies suggest a smaller glacial extent (and ice volume) than in stand-alone ice sheet models (forced with global mean sea level), as self-gravitational attraction and local RSL changes dominate, associated with this negative (self-stabilizing) feedbacks of the RSL (Gomez et al., 2013; de Boer et al., 2014, 2017). This complex interplay of solid Earth, sea level and ice
80 dynamics has therefore played a major role during glacial cycles (Whitehouse et al., 2019) ~~.~~ and is relevant for interpreting constraints on GIA in the periphery of the ice sheet, such as sea-level indicators and GPS uplift rates (Konrad et al., 2014).

~~Since~~ A global sea-level low stand was reached during the Last Glacial Maximum (LGM) ~~about 21~~between 26,500 and 19,000 years ago ~~(21) (Peltier, 2005), deglaciation of the AIS may have been initiated or amplified in periods of rapid sea level rise~~(26.5–19 kyr BP, Clark et al., 2009). The rapid sea-level rise since LGM due to the collapse of the northern hemisphere ice sheets likely contributed to the destabilisation of the AIS, as iceberg-rafted debris records in deep-sea sediments suggest (Weber et al., 2014; Jones et al., 2022). ~~Such~~ Accordingly this is reflected in an inter-hemispheric ~~sea level effects may have contributed to the~~ synchronicity of the large ice sheets~~during ice-age cycles (Gomez et al., 2020).'~~ changes (Gomez et al., 2020).

There is growing evidence that during the Holocene period (the past 11,700 years) the solid-Earth uplift in combination with ice rise formation may have caused the re-advance of the Ross Sea ~~grounding line~~ GL to present-day ~~location~~ position after an initial phase of rapid deglaciation ~~(Lingle and Clark, 1985; Kingslake et al., 2018; Johnson et al., 2022)~~(Lingle and Clark, 1985; Kingslake, while in the Amundsen Sea ~~grounding lines~~ GLs remained stable for the last 5,500 years until recently (Braddock et al., 2022). ~~This is a highly relevant information in defining the~~ The present-day state of the AIS, including its contemporary rates of change~~(Coulson et al., 2021). It characterizes~~, characterizes its stability and the potential for ~~sea level~~ sea-level rise in an increasingly warming climate (Joughin and Alley, 2011).

Ice sheet models have been coupled to GIA models with different levels of complexity ~~(de Boer et al., 2017; Whitehouse, 2018)~~ (de Boer et al., 2017; Whitehouse, 2018; Swierczek-Jereczek et al., 2023, see overview Table 1). The computationally efficient two-layer approach with an 'Elastic Lithosphere and a Relaxing Asthenosphere' (ELRA) accounts for the vertical bedrock adjustment for one given relaxation time (Brotchie and Silvester, 1969; Le Meur and Huybrechts, 1996) and is widely used in ice sheet modeling or coupled Earth system modeling (Pollard and DeConto, 2012; DeConto and Pollard, 2016; Pattyn, 2017; Quiquet et al., 2018). The local response time and flexural regidity can be also varied laterally (Coulon et al., 2021).

ELRA can be improved when the time-lagged mantle flow in the asthenosphere below an elastic thin plate is approximated by solving the corresponding biharmonic differential equation using Fast Fourier Transformation (Lingle and Clark, 1985; Bueler et al., 2007; Albrecht et al., 2020a; Book et al., 2022). In this 'Lingle-Clark' (LC) bed deformation model, a wavelength-depending response time spectrum replaces the single exponential decay parameter of the ELRA approximation. Hence, only the uniform mantle viscosity and flexural rigidity (or elastic lithosphere thickness) are used as input parameters valid for the considered half-space.

In addition to the bedrock changes, ~~commonly~~ global mean sea level anomalies are used as external forcing for ice sheet models to account for water depth changes at the ~~grounding line~~ GL (Goelzer et al., 2020). The LC model is limited to a certain region (e.g. Antarctica) and is unable to prescribe gravitational, globally self-consistent water-load changes or to account for feedbacks associated with polar motion due to GIA. The computationally inexpensive approach has been recently extended by considering lateral variations in Earth structure and a regional sea-level change (Swierczek-Jereczek et al., 2023).

In order to account for both global and near-field spatial ~~variablity of relative sea level~~ variability of relative sea-level change consistent with dynamic changes in ice sheet extent, coupled ice sheet–solid Earth models need to simultaneously solve the '~~sea level~~sea-level equation' (Farrell and Clark, 1976), as realized in 'Self-Gravitating ~~viscoelastic~~ Viscoelastic solid-Earth Models' ~~(SGVEM: e.g., de Boer et al., 2014; Gomez et al., 2015, 2020; Konrad et al., 2015; Coulon et al., 2021)~~(SGVEM: e.g., de Boer et al., 201

. GIA models generally account for both solid-Earth deformation and gravitational effects in combination with rotational effects in response to changes in the redistribution of ice and ocean masses (Milne and Mitrovica, 1996).

Most GIA models so far compute changes in Earth deformation and geoid for a radially varying (depth dependent) 1D Earth structure using spherical harmonics ~~(Whitehouse et al., 2012; Konrad et al., 2015; Pollard et al., 2017)~~(Whitehouse et al., 2012; Konrad et

. In regions of weak Earth structure, as for instance ~~presumably~~ in West Antarctica, the observed uplift rates are not compatible with the response of a viscosity structure usually applied for northern-hemisphere GIA in the range of 10^{20}–10^{21} Pa s and a lithosphere thickness of ≈ 100 km (Whitehouse, 2018; Ivins et al., 2023).

~~Recently,~~ Since the 2000s, 3D viscoelastic Earth models were developed (e.g. Martinec, 2000; Latychev et al., 2005; Wu et al., 2005; Zh and considered in a new generation of GIA models ~~accounts for the 3D Earth structure (A et al., 2012; van der Wal et al., 2015; Nield et al.,~~ ~~for a prescribed ice thickness (load) history.~~ (e.g. Klemann et al., 2008; A et al., 2012; van der Wal et al., 2015; Nield et al., 2018; Bagge et . Interactively coupled to ice sheet models, such 3D GIA models find significant differences in West Antarctic Ice Sheet (WAIS) evolution on glacial time scales compared to 1D GIA or standalone ice sheet models ~~(Gomez et al., 2018; Han et al., 2022; Van Calcar et al.,~~ (Gomez et al., 2018; Han et al., 2022; Van Calcar et al., 2023; Swierczek-Jereczek et al., 2023). The underlying coupling methods all imply a similar iterative process to account for the unknown initial bed topography, but differ with respect to the coupling time steps ~~in the respective approaches~~ ranging from hundreds to thousands of years.

Here, we present a set of new simulations of ~~Antarctic Ice Sheet~~ AIS evolution over the last 246,000 years (i.e. two full glacial cycles) with the Parallel Ice Sheet Model (PISM) coupled to the VIscoelastic Lithosphere and MAntle model (VILMA) solving for GIA.

2 Methods

2.1 PISM

The Parallel Ice Sheet Model ~~(PISM[1], here based on v1.2.2)~~(PISM User Manual, 2023, here based on v1.2.2, see also Section 'code and da , is an open-source [1] three-dimensional ice sheet model ~~(Winkelmann et al., 2011; PISM User Manual, 2023)~~(Winkelmann et al., 2011; The , written in C++ programming language. PISM has been previously applied in glacial-cycle simulations (e.g. Golledge et al., 2014; Sutter et al., 2019; Albrecht et al., 2020a, b), and can be easily coupled to other climate or Earth system model components (e.g. Kreuzer et al., 2021; Ziemen et al., 2019; Yang et al., 2022).

We here use a hybrid combination of two stress-balance approximations for the deformation of the ice, the Shallow Ice – Shallow Shelf Approximation ~~(SIA-SSA Hindmarsh, 2004)~~(SIA-SSA, Hindmarsh, 2004), that guarantees a smooth transition from vertical-shear dominated flow in the interior via sliding-dominated ice stream flow to fast plug flow in the floating ice shelves (Bueler and Brown, 2009), while neglecting higher-order modes of the flow. Driving stress at the ~~grounding line~~ GL is discretized using one-sided differences (Feldmann et al., 2014). ~~Using a sub-grid interpolation scheme (Gladstone et al., 2010),~~ ~~the grounding line location~~ The GL position simply results from flotation condition, without additional flux conditions imposed

---

[1]~~, see also Section 'code and data availability'~~

[1]

(Reese et al., 2018c). Basal friction and basal melt ~~is interpolated accordingly (Seroussi and Morlighem, 2018; Hewitt and Bradley, 2023)~~ are interpolated according to a linear sub-grid interpolation scheme (Gladstone et al., 2010; Seroussi and Morlighem, 2018; Hewitt and Bra . Thus, ~~grounding-line~~ GL migration is reasonably well represented in PISM (compared to Stokes flow), even for coarse reso-
lution (Pattyn et al., 2013; Feldmann et al., 2014).

Ice deforms according to the Glen-Paterson-Budd-Lliboutry-Duval flow law with exponent $n = 3$ ~~.~~ (Lliboutry and Duval, 1985). PISM simulates the three-dimensional polythermal enthalpy conservation for a given surface temperature and basal heat flux and thus captures melting and refreezing processes in temperate ice (Aschwanden and Blatter, 2009; Aschwanden et al., 2012). It is solved on a 3-dimensional grid with 81 vertical layers, with 20 m resolution at the base. The energy conservation scheme also accounts for the production of sub-glacial (and transportable) water (Bueler and van Pelt, 2015), which affects basal friction via the concept of a saturated and pressurized sub-glacial till. The till friction angle, which accounts for characteristics of the underlying substrate, has been optimized for present-day ice flow (Albrecht et al., 2020a). Depending on the resultant yield stress this allows for grow-and-surge instability (Feldmann and Levermann, 2017; Bakker et al., 2017; Schannwell et al., 2023). Here we use the non-conserving hydrology model, where the till water content in each grid cell is balanced by basal melting and a constant drainage rate.

~~ice~~ Ice shelf margins can evolve up to the edge of the continental shelf (here defined at 1800 m depth) constrained by a terminal thickness criterion (>75 m). Iceberg formation from ice shelves is parameterized based on spreading-rates (Levermann et al., 2012). Ice shelf melting is calculated using the Potsdam ice shelf Cavity mOdel (PICO) that considers basin-mean ocean properties on the continental shelf in front of the ice shelves and mimics the vertical overturning circulation in the ice shelf cavity (Reese et al., 2018a).

PISM comes with a generalized version of the Lingle-Clark bedrock deformation model (Bueler et al., 2007), assuming an elastic lithosphere, a resistant asthenosphere and a viscous half-space below (Whitehouse, 2018). The LC model is computationally efficient, the default coupling time step is 10 yr, but it does not account for regional ~~sea level (geoid) variations~~ sea-level variations due to gravitational attraction of the ice as of the deforming solid Earth.

A continental-scale representation of modern Antarctic bed and ice sheet topography is obtained from the Bedmap2 dataset (Fretwell et al., 2013). We simulate the entire Antarctic continent with 16 km grid resolution (381×381 regular grid size) compatible with the definition of the initMIP and ISMIP6 model intercomparison project (Nowicki et al., 2016, 2020). With an adaptive explicit time stepping of around 0.34 ± 0.03 yr, one glacial cycle (123 kyr) can be simulated within 1–2 days wall clock time with 64 CPU cores on a standard memory computing node [1] ~~(~~at DKRZ (see https://docs.dkrz.de/doc/levante/configuration.html, last access: 05 June 2024, 'AMD 7763' with 128 CPU cores in total, 256 GB main memory and 2.45 GHz base clock).

2.2 VILMA

The VIscoelastic LIthosphere and MAntle model (VILMA) solves the field equations for an incompressible self-gravitating viscoelastic sphere in the Lagrange domain, laterally in spherical harmonics, radially with finite elements, and in time using

---

[1]

180   an explicit time-differencing scheme assuming a Maxwell rheology as material law. Lateral variations in viscosity are considered as shear energy perturbations, which are calculated on a Gauss-Legendre grid in the spatial domain and which are transformed back into the spectral domain at each time step (for details see Martinec, 2000). The code has been benchmarked for a spherical symmetric Earth structure (Spada et al., 2011), i.e. for a 1D Earth structure, and was applied in studies accounting for lateral variations, i.e. for a 3D Earth structure (Klemann et al., 2008; Bagge et al., 2021). Furthermore, the effect of rotational feedback is accounted for (Martinec and Hagedoorn, 2014), following the discussion in Mitrovica et al. (2005).

    The sea-level equation, describing the gravitationally consistent and mass-conserving redistribution of ice masses and ocean water (Farrell and Clark, 1976; Mitrovica and Milne, 2003; Kendall et al., 2006), is solved in the spatial domain (Hagedoorn et al., 2007) and was benchmarked in Martinec et al. (2018). Coast lines can freely migrate according to the local RSL. The loading effect of floating versus grounded ice is accounted for. The GL position is determined by the flotation conditions and hence by densities of ice and ocean water (consistent with PISM). The GL migration is associated with a redistribution of water mass between ice sheets and ocean, which can result in large non-uniform near-field RSL patterns (Mitrovica et al., 2001; Spada et al., 2013).

195   For the radial discretization, we chose $\Delta z = 5\,\mathrm{km}$ down to $420\,\mathrm{km}$ depth, followed below by $\Delta z = 10\,\mathrm{km}$ down to $670\,\mathrm{km}$ and $\Delta z = 40$ to $60\,\mathrm{km}$ down to the core–mantle boundary, where the parameterisation of the elastic shear modulus and density structure follows the Preliminary Reference Earth Model (PREM, Dziewonski and Anderson, 1981). The interaction with the fluid core is considered as a boundary condition, confining the solution domain to the Earth's crust and mantle. The spectral resolution is set to Legendre degree and order 170, meaning that layers with lateral variations are discretized on a 256×512 (n128) grid corresponding to a wavelength of $\sim 120\,\mathrm{km}$. The grid size is based on an alias-free condition, which defines the numbers of latitudinal Gauss-Legendre points to be larger than 3/2 of the maximum Legendre degree considered (e.g. Martinec, 1989). We consider this as sufficient due to the general low-pass response of the Earth to surface loading and the spectral resolution of the considered tomographic model of only degree 63 (Steinberger, 2016). Higher resolutions were tested in this project, but did not show significant changes (see Sect. 3.1). The sea-level equation, defining the gravitationally-consistent mass redistribution between oceans and ice sheets in response to the deforming solid Earth, is solved in the spatial domain, also on a Gauss-Legendre grid, but with a significantly higher resolution of 1024×2048 (n512) corresponding to a wavelength of $\approx 30\,\mathrm{km}$.

    In order to allow for restarts, the original Fortran77 code was modularized and in main parts extended using Fortran90 commands during the PalMod project (see acknowledgements), and OpenMP parallelization (OpenMP, 2012-2023) was implemented explicitly. In our coupled simulations, VILMA uses explicit time steps of $2.5\,\mathrm{yr}$, in order to be able to solve also for very low mantle viscosities at the order of $10^{19}\,\mathrm{Pa\,s}$. Considering this set up, one glacial cycle

---

[1]

(123 kyr) can be simulated within 19 h wall clock time with 64 CPU cores on a standard memory computing node (same as indicated for PISM).

215 ## 2.3 PISM-VILMA Coupling

PISM and VILMA are offline-coupled using a coupling time step that can be rather short ~~(and is only limited by the explicit time step chosen in VILMA and PISM. As default, we apply a coupling time step of~~ $\Delta t =$ 100 yr~~as default). This is an advantage of the explicit time stepping and the weak formulation (in time-domain)of the solid-Earth dynamics (Martinec, 2000) in contrast to the normal-mode approach (in Laplace domain) used by most of the~~, at which PISM and VILMA exchange data. The

220 strategy, where ice load and relative sea level are exchanged (see below), was already applied in studies with an older version of VILMA coupled with dynamic ice sheet models RIMBAY and PSUICE-3D (Konrad et al., 2014, 2015, respectively), and also in the Earth system model CLIMBER-X (Willeit et al., 2022), where the current VILMA version was coupled directly to SICOPOLIS as a fortran module. Here, for the first time the 3D feature of VILMA is applied, whereas in the former studies only a 1D Earth ~~models (e.g. Peltier, 1974).~~ was considered.

225 In a first step, PISM runs for the coupling interval (from t_0 to t_1), based on the initial bed elevation, which remains constant over ~~this~~ the coupling time step Δt (see Fig. 2). Subsequently, VILMA integrates over the same interval (from t_0 to t_1) according to a global ice sheet load history, which combines ICE-6G_C (Peltier et al., 2015) north of 60°S and the PISM-simulated AIS changes south of 60°S, remapped to the VILMA grid. VILMA interpolates the ice sheet history between the snapshots at beginning and end of the coupling interval and provides the global change in RSL at predefined snapshots. The

230 RSL at t_1 is (bilinearly) remapped back to the PISM grid.

Then, this process restarts for the next coupling interval (t_1 to t_2). PISM interprets the RSL change as negative vertical displacement of the bed elevation with respect to a reference surface elevation (geoid), or as change in water depth, if the bed elevation has negative values. That means, the surface elevation of the ocean in the PISM simulations remains at $z = 0$. With the adjusted bed topography (water depth), the ice sheet's ~~grounding line~~ GL can move directly due to the flotation criterion

235 or indirectly due to induced ice dynamical changes. These changes in the ice ~~and water~~ load are then passed to VILMA again, which simulates the same coupling ~~interval~~ time step (from t_1 to t_2), before PISM simulates for the next coupling interval.

In our coupling scheme, the PISM response always ~~lacks~~ lags behind the VILMA step by one coupling step, i.e. RSL change from t_{i-1} to t_i calculated in VILMA is only reflected in ice dynamics in PISM from t_i to t_{i+1}. The implied numerical error remains small if short coupling time steps are used (see sensitivity to coupling time step in Sect. 3.1). We do not make use

240 of (internal) iterations within a (longer) coupling time step as suggested, e.g., by Van Calcar et al. (2023), even though this could be easily implemented in PISM-VILMA. Furthermore, we avoid extrapolation of sea level and bed elevation changes to the next coupling interval as in Konrad et al. (2015), which principally can cause numerical instabilities. We also do not pass the sub-grid information of ~~grounding line~~ GL interpolation, used in PISM for the basal friction, to VILMA. In case of ~~grounding line~~ GL migration, this could avoid ad-hoc load changes from single grid cells. Our python coupler [1] pismvilma

---

[1]
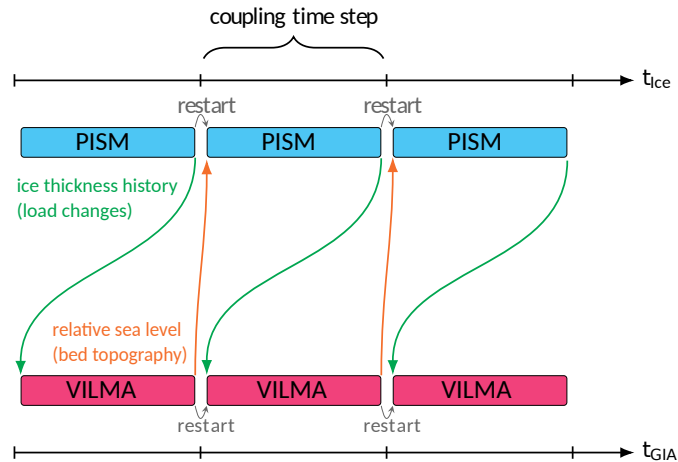
Figure 2. PISM-VILMA coupling scheme, adopted from Kreuzer et al. (2021).

(Albrecht, 2024) uses CDO and NCO tools [1] (CDO; NCO, 2003-2024) for remapping two-dimensional RSL changes from the global Gauss-Legendre grid used in VILMA to the Antarctic Polar Stereographic [1] Maptiler (2024) equidistant Cartesian grid used by PISM ~~, and~~and, vice versa, Antarctic ice thickness from the PISM grid back to the global VILMA grid.

On a High Performance Computing (HPC) system with a 'slurm' batch queue system, we make use of the heterogeneous job support [1],(SLURM, 2003-2024), which can simultaneously optimize for the openMP [1] ~~parallelization~~ parallelization (OpenMP, 2012-2023) on a single compute node (in case of VILMA and the python coupler) and the MPI parallelization that can be utilized across multiple compute nodes (in case of PISM). The remapping takes about 23% of computational time for 10-yr coupling time step, 9% for 100 yr and only 1.5% for 1000- yr, when using 3D Earth structures (see PISM2VILMA and VILMA2PISM in Table 1). Total computation time for simulating 1 kyr on a standard memory computing node (128 cores in total, see details in Sect. 2.1) is about 25 min for the 1000 yr coupling time step (25 CPUh), 30 min for 100 yr (35 CPUh) and 100 min for 10 yr (100 CPUh), when using 64 CPU cores for VILMA, PISM and the remapping. Considering only 1D (radial) Earth structures in VILMA brings a speed-up by a factor of 5 for the VILMA step and hence of almost 50% speed-up in the coupled model performance, for coupling time steps of 100 yr.

For comparison, Van Calcar et al. (2023) used a 3D GIA finite-element model with 16 CPU cores to simulate the last glacial cycle, with coupling time steps between 5000 and 500 yr, 40 km resolution in the ice sheet model and between 30 and 200 km in the GIA model, showed a performance of 16 CPUh per 1 kyr. However, when internal iterations were considered, the coupled model system required about 120 CPUh per 1 kyr.

In order to account for (long) memory effects of the AIS to the climate history, we run the coupled simulation for two full glacial cycles (246 kyr, see Fig. 3 a), with the northern hemisphere described by the ICE-6G_C reconstruction (available for

---

[1] ~~;~~
[1]
[1]
[1]

step	100×10 yr	10×100 yr	1×1000 yr
PISM	2876 (49.7%)	1078 (52.2%)	999 (60.3%)
PISM2VILMA	871 (15.1%)	141 (6.8%)	19 (1.1%)
VILMA	1581 (27.3%)	802 (38.9%)	632 (38.2%)
VILMA2PISM	459 (7.9%)	43 (2.1%)	7 (0.4%)
TOTAL	5788 (1.60 h)	2063 (0.57 h)	1657 (0.47 h)

Table 1. Mean wall clock time for PISM-VILMA steps in seconds (and %) for 1 kyr simulation for the reference 3D Earth structure with 64 CPU cores and different coupling time steps, run on Levante (DKRZ). All three coupled simulations used the reference spatial resolution of n512 for the sea level equation in VILMA, n128 for the viscoelastic deformation in VILMA and 16 km for PISM in the Antarctic domain.

the last ~~123~~122 kyr, repeated for the penultimate glacial cycle ~~while smoothed~~ with a time shift by 124 kyr and concateneted
at the Last Interglacial), similar to Han et al. (2022). For consistency, the climatic and ocean forcings are applied as described
in previous PISM standalone simulations (Albrecht et al., 2020a), which have been coupled to the LC bed deformation model
(Bueler et al., 2007). In order to support an earlier deglaciation around 15 kyr BP (see Fig. 3 b) ~~, which provides~~ providing
a better match with paleo proxies (Briggs and Tarasov, 2013; Albrecht et al., 2020b), PISM parameters ~~are~~ were slightly
adjusted in this study ~~slightly adjusted~~ (e.g. till water drainage rate or precipitation scaling). Simulations are run until the
year 1950 (corresponding to 0 kyr BP), such that the recent anthropogenic warming is ignored in the ~~climate forcing with
ice core reconstructions (here a combination of EPICA Dome C and WAIS Divide ice core, cf. Albrecht et al., 2020a)~~ice-core
reconstruction based climate forcing (here a combination of EPICA Dome C and WAIS Divide ice core, see Albrecht et al., 2020a)
.

For the initial global bed topography we apply the present-day ETOPO1 [1] bathymetry (Amante and Eakins, 2009), updated
with Bedmap2 (Fretwell et al., 2013) in the Antarctic sector. As the initial bed topography of the simulation (at 246 kyr BP) is
not known a priori, we iterate several times over the period of two glacial cycles ~~(Kendall et al., 2005)~~(Kendall et al., 2005; Van Calcar et al.
, and successively correct for the initial bed topography according to the mismatch of the present-day bed topography to obser-
vations from Bedmap2 of the previous iteration (compare Fig. 3 and Fig. 4). Ideally, the present-day RSL subtracted from the
initial bed topography should converge to the present-day topography. In the first iteration, the present-day RSL is underesti-
mated by up to 100 m in East Antarctica (bedrock too high) and overestimated by up to 100 m in West Antarctica (Fig. 4a). As
measure of the mismatch we use the Root Mean Squared Error (RMSE) over the Antarctic computational domain. Generally,
the RMSE reduces with each iteration by a factor of 0.2–0.4 (see Fig. 3 c). We stop iterating when the RMSE falls below
the acceptance level of 10 m (dotted line). This iterative procedure aims at minimizing deviations from the present-day bed
topography, but we also find convergence of the present-day ~~sea level equivalent~~ Antarctic ice volume against observations
(Fig. 3 b); ~~although~~ nevertheless in some regions the misfit in ice thickness remains comparably high (Fig. 4g–l). In order to
convert Antarctic ice volume change in more practical units for better comparison, we here use the 'volume above flotation'

---
[1]
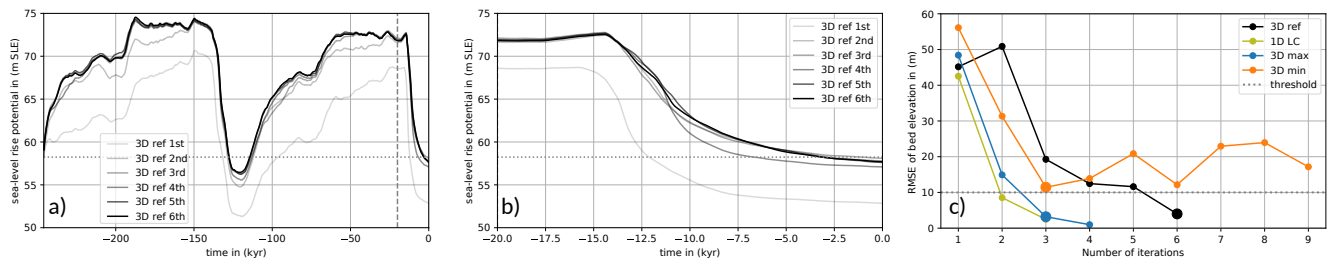
Figure 3. ~~PISM sea level relevant Antarctic ice volume~~ **Sea-level rise potential in coupled PISM-VILMA simulation** over a) 246 kyr ~~a)~~ and b) over the last 20 kyr ~~b)~~ showing convergence for six subsequent iterations ~~of coupled simulations~~ with reference 3D Earth structure ('3D ref') at n128 resolution and n512 resolution for the ~~sea level~~ sea-level equation. In each iteration the initial bed topography is adjusted, such that the misfit of present-day bed topography according to VILMA is minimized. c) ~~Ice volumes above flotation have been calculated considering cell-area weighting and density correction (Goelzer et al., 2020) with a temporal resolution~~ Root-Mean-Squared Error of ~~100~~ present-day bed topography anomalies in subsequent iterations for four different Earth structures, see Sect. 2.4 and Sect. 3.3. Big markers indicate last iteration selected for further comparison.
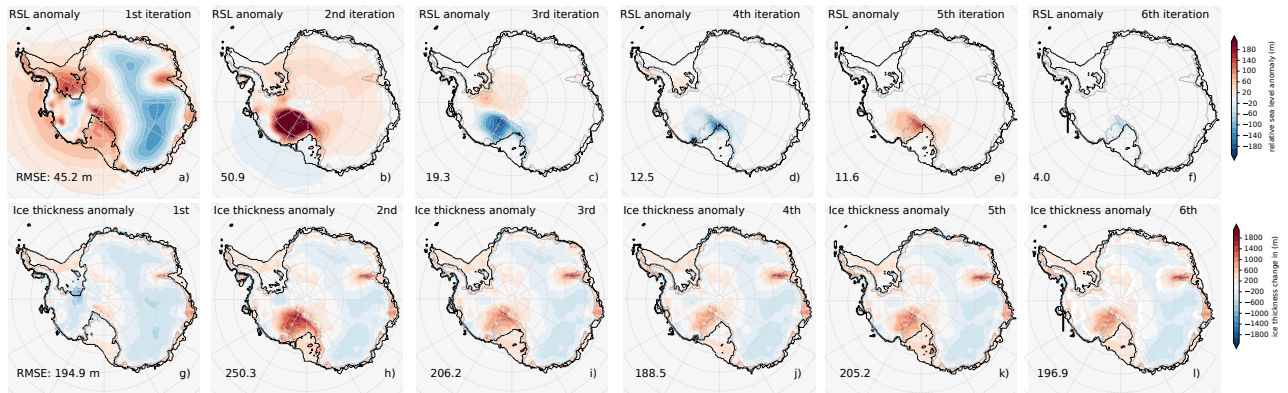
Figure 4. Anomalies of RSL (VILMA) and ice thickness (PISM) at present-day compared to Bedmap2 ~~bedrock~~ bed elevation and ice thickness observations (Fretwell et al., 2013), for six iterations of coupled glacial cycle simulations with reference 3D Earth structure (~~n128~~ ~~and sea level equation (n512~~ '3D ref', see Sect. 2.4), converging from 46 m RMSE to about 4 m RMSE for RSL anomaly (negative bed topography anomaly, cf. black points in Fig. 3c). This iterative procedure does not optimize for the present-day ice thickness. The iterations show a convergence with alternating sign in the mean RSL anomaly, particularly in the Siple Coast region in the Ross Sea sector. Black lines indicate modeled GL and ice shelf extent, grey is the observed GL.

approach with corrections for the density and in regions grounded below sea-level (Adhikari et al., 2020, Eq. 10). We apply this approach to the projected regional ice model domain using cell-area weights and a constant ocean area of 362.5 million km^2. Compared to an ice free state with present-day bed topography, this conversions provides a global mean estimate of the 'sea-level rise potential' (SLRP) in units of m SLE. As vertical land motion is already included in our RSL variable, we do not explicitly account for the 'water-expulsion effect' in the conversion (Goelzer et al., 2020; Pan et al., 2021).

290

2.4 Solid-Earth structures

~~In previous PISM simulations, the LC model (Lingle and Clark, 1985; Bueler et al., 2007) has been coupled every 10 to account for the viscoelastic displacement of the bedrock topography, assuming an elastic plate (with a flexural rigidity of 5×10^{24} ,~~
~~corresponding to a lithosphere thickness of 88) overlying a viscous half-space (with the upper mantle viscosity of 5×10^{20}). However, this approach is limited to a certain region (e.g. Antarctica) and is unable to solve self-consistently for sea level changes while considering a globally conserved water budget.~~

~~In VILMA not only vertically varying Earth structures (1D) can be considered, but also lateral changes in viscosity. Between~~ Between the West and East Antarctic plates, differences in the ~~viscosity of the upper mantle at about~~ upper-mantle viscosity, here shown at 280 km depth, can exceed two orders of magnitude (~~see~~ Fig. 5b). Based on seismic tomography models and geodynamical constraints, a dataset for the 3D Earth structure (including the lithosphere thickness) has been optimized such that the VILMA response minimizes the misfit to a global compilation of ~~relative sea level~~ RSL records (Bagge et al., 2021). According to their global investigation the 3D viscosity is bounded below by 10^{19} Pa s, which keeps integration time manageable for glacial cycle simulations. We do not modify the 3D Earth structure in view of geodetic inferences as these discuss recent load changes in specific Antarctic regions (e.g. Nield et al., 2014; Barletta et al., 2018), which are not the scope of this study. In the following we refer to the Class-I-type ('v_0.4_s16') as our reference 3D Earth structure ('3D ref').

In order to test for the effects of low and high ~~viscosity~~ viscosities on the ice sheet dynamics and to investigate possible feedbacks we define end member Earth structures of the laterally varying reference 3D Earth structure, '3D ref'. The '3D min' and the '3D max' take the minimum and maximum of '3D ref' over the Antarctic ~~regions~~ region south of 60°S at each depth interval (see Fig. 5a), respectively. The inferred minimum or maximum define a laterally uniform 1D Earth structure within the Antarctic region, while north of 60°S we consider the original '3D ref' structure, as we want to avoid far-field effects induced by changes in the northern hemisphere Earth structure. This implies a very thin lithosphere thickness of only a few kilometers and upper-mantle viscosities down to 10^{19} Pa s in the '3D min' case for Antarctica, while in the '3D max' case, the lithosphere thickness is around 130 km and upper-mantle viscosities remain larger than 4×10^{20} Pa s for all depth intervals (Fig. 5c).

3 Results

3.1 Sensitivity of ~~Antarctic Ice Sheet~~ AIS deglaciation to spatial resolution and coupling time step

The coupling time step is an important parameter in a coupled model system. As ~~in our coupling scheme,~~ PISM responds to changes in ~~relative sea level~~ RSL from VILMA of the previous time step, the coupling time step should be short enough to avoid delay effects~~of this asynchronicity~~. However, computational costs for the remapping of the ~~data~~ spatial fields and the initialization of each of the model steps occur at each coupling time step (cf. Table 1). A reasonable coupling time step therefore balances costs and accuracy.

We evaluate the sensitivity of the coupled simulations to coupling time steps Δt of 1000, 100 and 10 yr by comparing the deglacial response of the ~~Antarctic Ice Sheet~~ AIS over the last 20 kyr~~in terms of sea level equivalent ice volume (in units of).~~
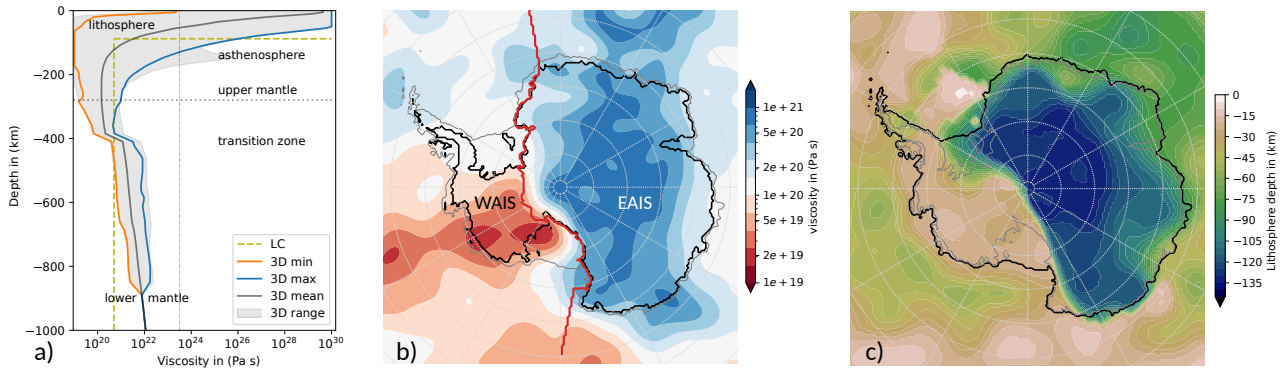
Figure 5. VILMA Earth structure. a) Vertical profiles ~~of viscosity~~ down to 1000 km depth for 3D Earth structures, with global ~~log-mean~~ logarithmic mean and range (grey), the Antarctic wide range (between orange and blue defining '3D min' and '3D max', respectively) and the two-layer profile as used in the Lingle-Clark model (olive). b) '3D ref' at 280 km depth (horizontally dotted line in a), showing a lateral variability of two orders of magnitude ~~in viscosity~~ (10^{19}–10^{21} Pa s). Present-day grounding line and calving front (Bedmap2 contours from Fretwell et al. (2013), grey and black respectively), and Zwally et al. (2012) drainage basin divide (red) between WAIS (basins 2–17) and East Antarctica (basins 18–27 and 1). **c**) Lithosphere depth defined by $10^{23.5}$ Pa s threshold (vertical dashed line in a), showing a thin lithosphere (< 50 km) in West Antarctica and a thick lithosphere exceeding 130 km in East Antarctica.

In all three cases we find a similar ~~sea level relevant ice volume~~ SLRP at LGM (in our simulations around 15 kyr BP) of around
325   ~~72~~72.5 m SLE, which is about 14 m SLE above the ~~present~~ present-day level (see Fig. 6a). At the onset of deglaciation, around 14 kyr BP, we find small discontinuities in the response for the largest coupling time step (blue ~~), at which~~ lines), as PISM responds to changes in bed topography ~~with~~ that remain constant for the 1000 yr ~~delay. This is mostly~~ interval, while the far-field RSL changes dramatically during 'meltwater pulse 1A' (MWP-1a). In fact, this is partly a consequence of the diagnostic calculation of the ~~sea level equivalent ice volume (above flotation) that also accounts for~~ SLRP, since changes in bed elevation also
330   affect the flotation height and hence potential sea-level contributions. The blue-solid line would be much smoother when total ice mass or grounded ice volume over time were shown. Interestingly, compared to $\Delta t \leq 100$ yr, we find during Holocene until present ~~we find slightly smaller ice volumes~~ day slightly smaller SLRP (by about 1 m SLE) for $\Delta t = 1000$ yr. ~~The~~ In case of a linear extrapolation of the RSL change rate in the PISM step for this Δt ~~(blue dashed) shows~~ blue-dashed line in Fig. 6a) we find a similar effect during deglaciation, with slightly earlier deglaciation than without extrapolation. Comparing the ice sheet response for ~~100~~$\Delta t = 100$ yr ~~(default) and 10~~and 10 yr~~coupling time steps, we find~~, we see only little differences for the
335   given spatial resolution of n512/n128 in VILMA and 16 km in PISM, which we interpret as 'convergence'. It should be noted, that the coupled system is highly non-linear with a high sensitivity to initial conditions. Convergence should be considered with respect to a certain range of internal variability (Albrecht et al., 2020a).

As total computational costs per modeled kyr decrease by about 20% between 1000~~and 100~~ yr and 100 yr~~coupling time step~~, but by about 65% between 100 yr and 10 yr~~coupling time step~~, we choose ~~a 100~~$\Delta t = 100$ yr ~~coupling time step~~as the
340   default ~~choice~~coupling time step for further experiments.

A recent study on time stepping and RSL precision (Han et al., 2022) with the coupled ice sheet–sea level model system of Gomez et al. (2013, 2020) suggests coupling time steps of at least 200 yr, while a previous coupled model study with coarser spatial resolution claimed that 1000 yr would be sufficient (de Boer et al., 2014). Coupling time steps of 500 yr are shown to

345   yield accurate ~~coupled~~ results, when using internal iterations and linear interpolation over the coupling time step (Van Calcar et al., 2023). Idealized experiments performed with a coupled model framework with VILMA chose 50 yr (Konrad et al., 2015). In fact, an optimal temporal resolution is highly linked to the spatial resolution and the involved Earth structure.
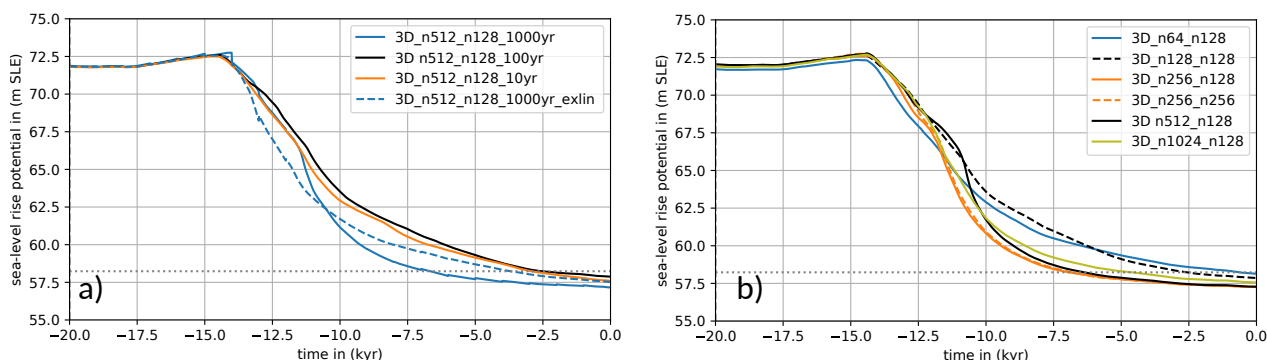
Figure 6. ~~Sea level relevant Antarctic ice volume over last 20 kyr for different coupling time steps and different spatial resolutions.~~ **Sea-level rise potential from Antarctica over last 20 kyr for different coupling time steps and different spatial resolutions.** a) Default coupling time step is 100 yr (black). Higher temporal resolution with 10 yr is shown in orange. Lower temporal resolution with ~~a~~ 1000 yr is shown in blue, and with linar extrapolation ('exlin') of RSL change rate in ~~blue dashed~~ blue-dashed. Here, all simulations were restarted from the ~~default~~ same restart state at 20 kyr BP ('3D ref', 6th iteration ~~)~~ with default spatial resolution). Shown time series have a resolution of 10 yr. b) Reference spatial resolution is n512 for the ~~sea level~~ sea-level equation in VILMA, n128 for the viscoelastic deformations and 16 km in PISM (black). Higher spatial resolution for the ~~sea level~~ sea-level equation is shown in olive (n1024), ~~coarse~~ coarser resolution in blue (n64), ~~black dashed~~ black-dashed (n128) and orange (n256). In ~~orange dashed~~ orange-dashed, also the resolution for the viscoelastic deformations ~~in VILMA~~ has been increased to n256. All simulations have been initiated from the ~~default~~ same initial state at 246 kyr BP (4th iteration). The coupling time step and temporal resolution of the plotted time series is 100 yr. PISM resolution has not been varied here.

There are interactive processes between ice sheets, ocean and the solid Earth that need sufficient spatial resolution to be adequately resolved, in particular in the grounding zones of marine ice sheets. The default spatial resolution in our coupled

350   simulations is 16 km in the ~~Antarctic Ice Sheet~~ AIS and 0.2° for the global ~~sea level~~ sea-level equation (n512), which corresponds to 20 km in latitude and to about 6 km in longitude at 71°S. The viscoelastic deformation is resolved with 0.7° (n128), which corresponds to about 78 km in latitude and 25 km in longitude at 71°S. A doubling in the viscoelastic resolution (n256) has only minor effects on the ~~Antarctic Ice Sheet~~ AIS deglaciation (see orange lines in Fig. 6b). A coarser spatial resolution in the ~~sea level~~ sea-level equation, however, delays deglaciation during the Holocene (~~blue and black dashed~~ blue-solid and

355   black-dashed lines for n64 and n128, respectively), with a SLRP difference of up to 2 m SLE ~~difference~~ compared to the reference resolution. These difference mainly result from RSL anomalies in the Ross Sea section (Fig. S 1). Only small differences

in ~~ice volume~~ SLRP are found at around 11 kyr BP for even higher spatial resolutions (cf. olive and black lines for n1024 and n512, respectively). The resolution of the ice sheet model has not been varied here, as this would require a new ensemble of simulations to constrain model parameters, as for the complex geometry of the AIS some parameters are resolution dependent (Albrecht et al., 2020a, b).

3.2 ~~Antarctic Ice Sheet~~ AIS build-up and deglaciation within bounds of reference 3D Earth structure

The reference 3D Earth structure ~~discussed in Bagge et al. (2021)~~ ('3D ref') discussed in Bagge et al. (2021) implies a large range of lithosphere thickness and mantle viscosity in key regions of the AIS. In order to evaluate ~~the ice-dynamical effects for variation of~~ effects of lateral variations in the underlying Earth structure on ice dynamics, we discuss changes in the grounded AIS area (~~grounding line~~ GL extent) and its ~~sea level equivalent ice volume~~ SLRP over the last ~~123~~246 kyr.

First, we consider the lower bound of '3D ref', i.e. '3D min' (Fig. 5a). In our coupled simulations with '3D min' (3rd iteration), the AIS holds about $14\,\mathrm{m}$ SLE more ~~ice volume~~ SLRP at the LGM (here at $15\,\mathrm{kyr}\,\mathrm{BP}$) than observed at present ~~(57.9±0.9 m SLE, Morlighem et al., 2020)~~day. This corresponds to a maximum LGM grounded ice ~~extent~~ area of 15.9 ~~mio.~~ million km^2 (Fig. 7b) and a total ice mass of 31.2 ~~mio.~~ million Gt, respectively. For the highly viscous '3D max', the ~~sea level relevant ice volume~~ SLRP at LGM reaches only $10\,\mathrm{m}$ SLE above present day, corresponding to 28.9 ~~mio.~~ million Gt and 15.1 ~~mio.~~ million km^2 grounded ice sheet ~~extent~~area. In both cases, the WAIS contributes 2–3 times more ice to the rising sea level since LGM than the East Antarctic Ice Sheet (EAIS) (Fig. S ~~2a~~4a). The largest differences in ice sheet response between '3D min' and '3D max' can be detected in the Ross and Ronne Ice Shelf basins and in the Bellinghausen and Amundsen Sea, where for '3D min' ~~the relative sea level~~ locally the RSL is up to $500\,\mathrm{m}$ higher (and hence the underlying bedrock deeper), leading to more extended and more than $1000\,\mathrm{m}$ thicker grounded ice (~~Fig~~cf. Figs. 8a, d and Figs. 8b, e, as '3D min' and '3D ref' have similar LGM extent). In Sec. 4, we will discuss this additional feedback mechanism that can explain enhanced ~~LGM grounding line advance~~ GL advance at LGM for weak Earth structures.

In the first iteration, without corrected initial bed topography, we find already similar differences of ~~Antarctic ice volume~~ AIS evolution over time for the different Earth structures, but generally 3–4 m SLE lower ~~ice volumes and lower ice sheet extents~~ SLRP (transparent lines in Fig. 7a, b) and smaller grounded ice sheet areas (transparent lines in Fig. S 2 b) than for the last iteration. During the iterations, bed topography and ~~ice volume~~ SLRP converge at present day towards their observed values (Fig. 3c). However, modeled grounding lines at present ~~tend to be slightly more extended than in observations (solid day~~ tend to slightly expand the observed grounded ice extent (solid and dotted lines in Fig. ~~7~~S 2 b).

The onset of deglaciation in our simulations occurs after ~~meltwater pulse 1A (MWP1a)~~ MWP-1a around $14.5\,\mathrm{kyr}\,\mathrm{BP}$ (Peltier, 2005), with a global mean sea level rise of about $20\,\mathrm{m}$ ~~in~~ during the following $350\,\mathrm{yr}$ (which corresponds to a mean rate of $50\,\mathrm{mm}\,\mathrm{yr}^{-1}$, see Fig. S ~~2b~~4b, c). This far-field effect, mainly in response to the northern hemisphere ice sheet losses (ICE-6G_C), reduces to about $10\,\mathrm{mm}\,\mathrm{yr}^{-1}$ between 14 and $7\,\mathrm{kyr}\,\mathrm{BP}$ (in total around $55\,\mathrm{m}$ of global mean sea level change) and partly compensates for near-field sea level drop in Antarctica, e.g. by viscoelastic bedrock uplift or gravitational attraction (see Figs. 8g, i at $10\,\mathrm{kyr}\,\mathrm{BP}$, cf. ~~Gomez et al. (2020)~~Gomez et al. (2020)). During the ~~period of~~ deglaciation until present-day we find a slightly slower decline, both in ~~ice volume~~ SLRP and grounded ice area for '3D min' compared to '3D max' (Fig. 7b
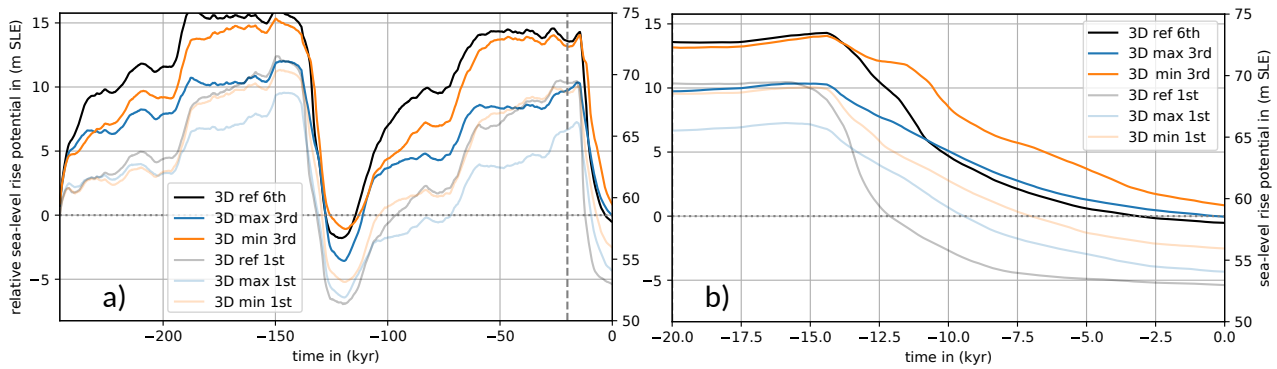
Figure 7. ~~Sea level relevant Antarctic ice volume and grounded ice area over last 123 kyr and over last 20 kyr for different Earth structures.~~ SLRP from Antarctica over last 246 kyr and over last 20 kyr for different Earth structures. Blue and orange lines show the response of the ~~Antarctic Ice Sheet~~ AIS in case of the '3D min' and '3D max' (cf. Fig. 5 a), which means respective 1D Earth structures south of 60°S and 3D further north. Black lines indicate the ~~ice sheet~~ SLRP response to '3D ref', i.e. 3D also at Antarctica. Transparent lines show the first iteration results with same initial topography; dotted horizontal line is present-day observation from Bedmap2 (Fretwell et al., 2013).

and Fig. S ~~1b~~2b). As their ~~LGM ice volumes~~ SLRP differ by around ~~34~~ m SLE at LGM, they provide different initial conditions at the onset of deglaciation. Grounding line retreat and ice sheet thinning (leading to ice shelf formation) can be slowed down if the isostatic rebound responds to these changes on rather short timescales. For '3D min', RSL change rates are in fact much higher than for '3D max', in West Antarctica reaching up to -500 mm yr^{-1} instead of -20 mm yr^{-1}, while in the far-field,

395   the RSL rises by about 10 mm yr^{-1} ~~(light orange shading , cf.~~ indicated by light-orange shading at the corners of the maps in Figs. 8g, i and Fig. S ~~2c~~4c, d~~)~~. This quick and rather localized response (e.g. Wan et al., 2022) defines a negative and hence stabilizing feedback on ~~grounding line retreat (cf. Wan et al., 2022)~~GL retreat (Gomez et al., 2010, 2012). For '3D min', rates of ~~ice volume change and grounding line retreat remain comparably high until present . As the~~ RSLP change and grounded ice area retreat remain almost constant at this comparably low level until present day. The viscoelastic rebound can take several

400   millennia for '3D max', and, in consequence, the stabilizing effect can be significantly delayed and it is active on a larger lateral extent. Over the last 3 kyr the AIS even ~~shows a slight tendency of grounding line re-advance~~ tends to readvance slightly (Fig. S ~~1b~~2b), as suggested in earlier studies (with PISM-LC) for rather high mantle viscosities of 5×10^{20} Pa s (Kingslake et al., 2018).

    The reference 3D Earth structure '3D ref' accounts for both, the weak Earth structure in West Antarctica and the higher

405   mantle viscosities and thicker lithosphere in East Antarctica (Fig. 5b, c). The corresponding response of the AIS for '3D ref' shows a similar ~~sea level equivalent ice volume (72~~SLRP (72.5 m SLE) and ice sheet area (15.8 ~~mio.~~ million km^2) at LGM as for '3D min' (Fig. 7b and Fig. S ~~1b~~2b, black and orange contour, respectively). The largest differences in the ice loads, compared to '3D max', are located in the West Antarctic region, where a rather low mantle viscosity and a thin lithosphere are dominant (Fig. 8a, d). The additional ice load causes further subsidence of the bedrock underneath, by up to 200 m more than

410 for '3D max' (Fig. S ~~3~~6), while in the adjacent coastal region the sea floor becomes about 50 m shallower than for '3D max'
(Fig. 8a, light blue shading). This feature is called 'forebulge' and results from lateral transport of displaced mantle material
and the flexure of the lithosphere. For '3D ref', ice loss rates can reach $1500\,\mathrm{Gt\,yr^{-1}}$ in the first millennia after the onset of
deglaciation (Fig. S ~~2f~~4f). This is slightly higher and also earlier than for '3D min' and generally higher than for '3D max'
($<500\,\mathrm{Gt\,yr^{-1}}$). Maximum bedrock uplift rates with up to $200\,\mathrm{mm\,yr^{-1}}$ are ~~possible~~ reached for the low-viscosity response in
415 West Antarctica (Fig. 8h), while maximum uplift rates below $50\,\mathrm{mm\,yr^{-1}}$ are associated with higher viscosities and a thicker
lithosphere in East Antarctica (Fig. S ~~2d~~4d and Video S 1).

At present ~~, the ice volume and~~ day, the SLRP, grounded ice area and ice mass for '3D ref' (6th iteration) converges against
~~57~~57.7 m SLE, 13 ~~mio.~~million $\mathrm{km^2}$ ~~,~~and 24.6 ~~mio.~~million Gt, respectively, which is close to observations (in our diagnostic:
~~57.8~~58.2 m SLE, 12.6 ~~mio.~~million $\mathrm{km^2}$, and 24.3 ~~mio.~~million Gt, dotted lines in Fig. 7a, b and Figs. S 2b, 3b).

420 ~~We have considered the upper and lower bounds of the reference 3D Earth structure in our coupled simulations ('3D max'~~
~~and '3D min'). As expected, the ice sheet~~ Counterintuitively, the SLRP response for '3D ref' ~~shows a trajectory in between~~
~~those~~ does not show a trajectory completely in between the two end members ~~. Furthermore~~'3D max' and '3D min'. Yet, the
coupled simulations reveal that in glacial periods of ~~grounding line advance the characteristics due to~~ GL advance the SLRP
trajectory evolves in a similar way as the trajectory for the weak Earth structure ('3D min')~~seem to dominate the overall ice~~
425 ~~sheet response~~, while in deglacial periods of ~~grounding line retreat the AIS response is dominated rather by the characteristics~~
~~of~~ GL retreat the SLRP from the AIS responds in a similar way as the trajectory for the stiffer Earth structure ('3D max').
The similarity of '3D max' and '3D ref' responses during deglaciation is even more pronounced for similar LGM ice sheet
conditions (ice sheet history until 20 kyr BP prescribed as in '3D ref', see ~~blue dashed~~ blue-dashed line in Fig. S ~~1a~~2a).

One important aspect to consider when using 'ice volume above flotation' as metric is that the bed elevation changes imply
430 changes in the grounded ice area and the converted potential sea-level contributions. Other metrics, e.g. the total ice mass, are
independent of bed elevation or sea-level changes. Figure S 3b shows that the differences in total ice mass evolution between
'3D ref' and '3D min' are reduced during glacial maxima. Another aspect is a cumulative effect of the performed iterations,
with shifted initial bed elevations depending on the present-day anomalies, and hence also on the LGM state and the rate of
deglaciation. In the first iteration all simulations are initiated with the same bed elevation and ice thickness distribution, such
435 that differences over time can be purely attributed to effects resultant from the different Earth structures (see transparent lines
in Fig. 7a and Figs. S 2b, 3b). With every iteration the differences in ice volumes/masses become larger for different Earth
structures, in particular during phases of glacial build-up.

3.3 Comparison to glacial-cycle simulations with the PISM-LC model

In order to discuss the impact of the more complete GIA model considered in the PISM-VILMA simulations, we run coupled
440 PISM-LC simulations with the global mean sea level (GMSL) change derived from a coupled simulation with a 1D Earth
structure (described in the next paragraph). The resultant GMSL timeseries is similar to the one obtained with '3D ref', as
well as to the global mean ICE-6G_C, obtained with 'VM5a' Earth structure (90 km lithosphere and 500 km thick upper
mantle with $5 \times 10^{20}\,\mathrm{Pa\,s}$), as in all cases the same ice thickness history for the northern hemisphere is used (cf. Fig. 9a and
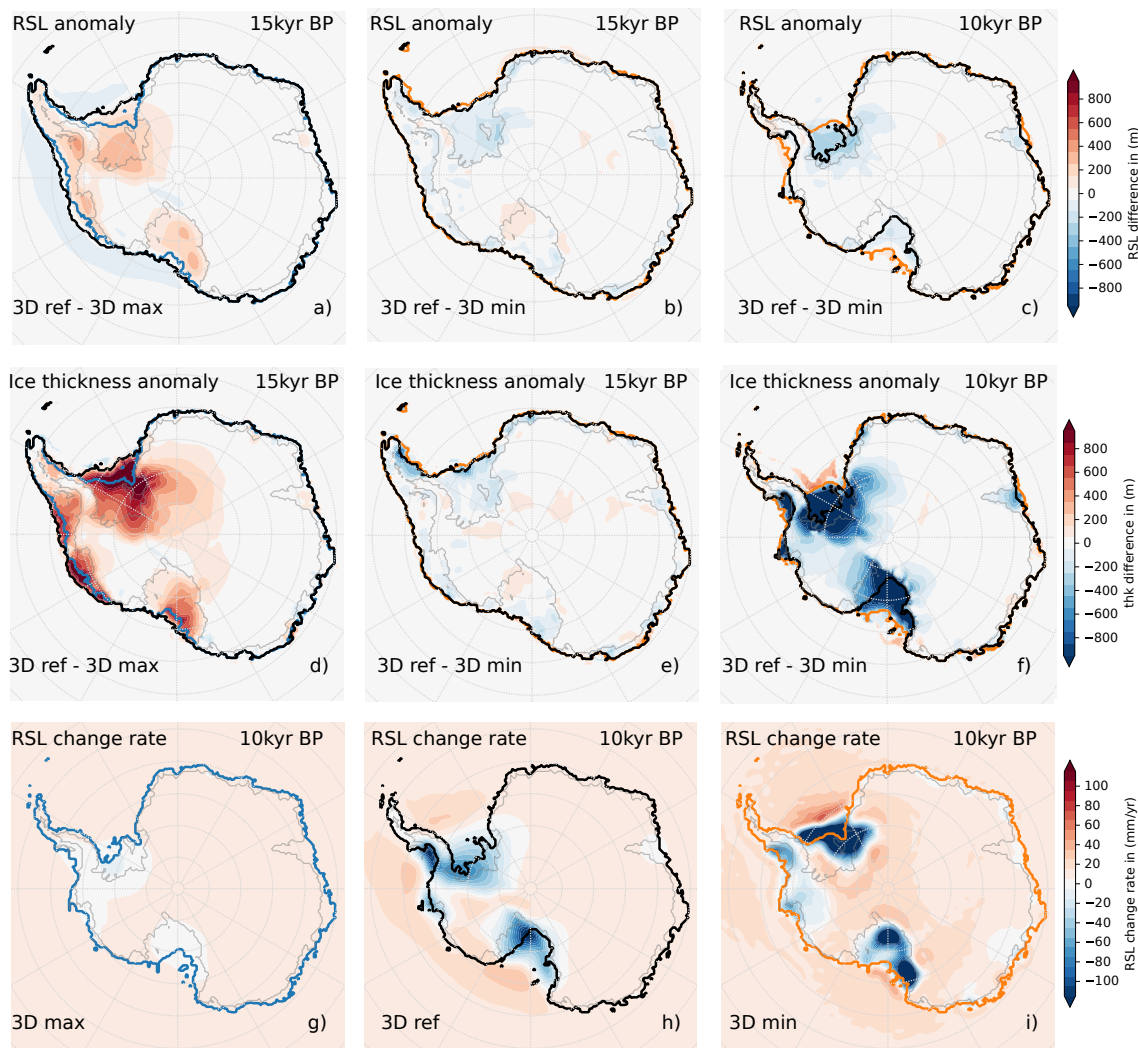
Figure 8. Difference in relative sea level (a–c) and ice thickness (d–f) for different Earth structures at 15 kyr and 10 kyr BP, and RSL change rates at 10 kyr BP for the different Earth structures (g–i). The modelled ~~grounding line~~ GL position due to the different Earth structures are shown as contour lines for '3D min' (orange), '3D max' (blue)~~and~~, '3D ref' (black) and at present day (grey).

Fig. S ~~2b~~4b). Note that in the PISM-LC coupling the change in ~~global mean sea level~~ GMSL is interpreted as a change in sea surface height. For the same PISM parameters and climatic forcing as in the PISM-VILMA simulations, we find after three iterations with PISM-LC a much lower ~~sea level relevant ice volume in~~ SLRP from Antarctica, with 59 m SLE at LGM (~~13~~13.5 m SLE lower than for '3D ref') and ~~56~~56.5 m SLE at present day (1 m SLE lower than for '3D ref') (olive vs. black in Fig. 9b). Differences in LGM ice volume mainly result from smaller ~~LGM grounding line extent~~ GL extent at LGM, especially in the Weddell Sea sector (Fig. S ~~3~~6). The PISM-LC results provide an estimate of the influence of GIA, although

450 the inferred LGM ice volume in Antarctica does not seem realistic. Previous model simulations, some of them scored against different paleo records, suggest that the ~~LGM ice volume~~ (uncorrected) SLRP at LGM in Antarctica was around 10 m SLE larger than at present ~~(see Fig. 11b in Albrecht et al., 2020b)~~day (cf. Fig. S 3a and see Fig. 11b in Albrecht et al., 2020b). For a slightly adjusted PISM parameter combination, a larger glacial ice sheet extent can be reproduced (Kingslake et al., 2018; Albrecht et al., 2020a).

455 If PISM-VILMA is run, analogous to PISM-LC, with a globally constant viscosity for the whole mantle of 5×10^{20} Pa s and a lithosphere thickness of 88 km (see Fig. 5a), we obtain lower ~~Antarctic ice volumes~~ SLRP from Antarctica than for '3D ref' (purple vs. black in Fig. 9b). In particular during glacial build-up the ~~Antarctic Ice Sheet volume~~ SLRP is about 10 m SLE smaller, at LGM around ~~7~~6.5 m SLE smaller (Fig. 9~~a~~, b). This is likely a consequence of the thicker lithosphere and the higher mantle viscosity in large parts of West Antarctica, ~~which also alters the global mean sea level (Fig. 9a)~~represented
460 in the simpler Earth model. Compared to the response from the PISM-LC simulations ~~, the Antarctic Ice Sheet volume~~ (olive line in Fig. 9b), the SLRP at LGM is about ~~6~~7 m SLE larger, likely a consequence of potentially stabilizing gravitational and rotational effects accounted for in VILMA. Regardless of the significant differences during glaciated periods, the present-day (and Last Interglacial) ~~ice sheet volumes~~ SLRP differ by less than 1 m SLE in these simulations (Fig. 9b), as the iterative procedure minimizes the present-day misfit in bed topography.
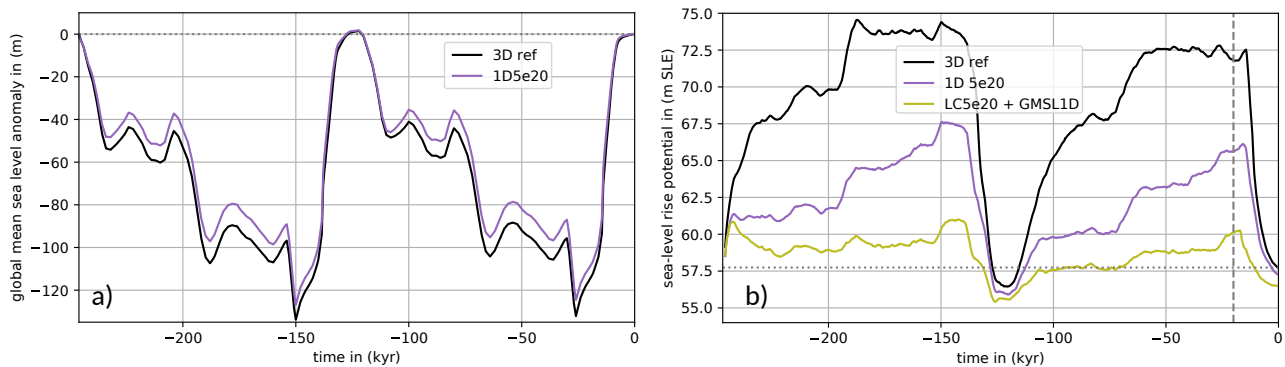
Figure 9. ~~Comparison of global mean relative sea level a) and sea level relevant Antarctic ice volume b) over last 246 kyr for Earth models of different complexity.~~ Comparison of global mean RSL a) and SLRP from Antarctica b) over last 246 kyr for Earth models of different complexity. Olive colored for the Lingle-Clark bed deformation model with 100-yr coupling time step, upper mantle viscosity of 5×10^{20} Pa s ('LC 5e20') and 88 km lithosphere thickness (5×10^{24} Nm flexural rigidity), suggesting a loss of about 3 m SLE ~~sea level contribution~~ in SLRP since LGM. Purple for the coupled PISM-VILMA model with 100-yr coupling time step, a 1D-Earth structure with 88 km thick elastic lithosphere and 5×10^{20} Pa s viscosity in the mantle below ('1D 5e20'). This simulation also solves for the ~~sea level~~ sea-level equation, yielding a ~~6~~7 m SLE larger contribution since LGM. The global mean of the sea level is used as forcing for the simulation with the LC model ('GMSL1D'). In black, the ~~Antarctic Ice Sheet~~ AIS response to the reference 3D Earth structure '3D ref' is shown with more than 14 m SLE change in SLRP since LGM~~is shown~~.

3.4 Far-field and near-field RSL effects on Antarctic deglaciation

In this section, we focus on the dynamics of the AIS in response to the northern hemisphere ice sheet's decay. We will provide an estimate of the far-field and near-field components of RSL change since LGM and compare our coupled simulation results with previous experiments in literature. Gomez et al. (2020) use a coupled ice sheet–GIA model that incorporates a global 1D (radially varying) viscoelastic mantle structure with four layers: a 50 km thick lithosphere, a 150 km thick low-viscosity zone of 10^{19} Pa s (representative for the weak Earth structure beneath the WAIS), an upper-mantle viscosity of 2×10^{20} Pa s and a lower-mantle viscosity of 3×10^{21} Pa s below 670 km depth (see Fig. S 7a). Like in our coupled simulations, Gomez et al. (2020) prescribe the northern hemisphere ice sheet history (ICE-5G, see anomaly at LGM in Fig. 10a), while the AIS evolution is simulated with a dynamic ice sheet model (PSU-ISM with 20 km resolution). Sea-level calculations are performed up to spherical harmonic degree 512, and coupled every 200 yr. Key differences are that PISM-VILMA uses a global 3D Earth structure and iterations are performed over the last two glacial cycles (246 kyr instead of starting at 40 kyr BP). On the one hand side we have to acknowledge a long memory in the ice sheet's thermal state of the order of 100 kyr (Briggs et al., 2013; Albrecht et al., 2020a). On the other hand the LGM ice volume depends on the previous glacial build-up and the rate of deglaciation depends on the LGM ice volume. The potential sea-level contribution from the AIS since LGM (here at 21 kyr BP) is considerably larger in our simulations (13 m SLE instead of 5 m SLE). In their coupled model setup, the simulated AIS volume changes since LGM suggest a rather low sensitivity to different radial 1D and 3D Earth structures (Pollard et al., 2017; Gomez et al., 2018).

In our coupled PISM-VILMA simulations, maximum LGM sea level fall of more than 400 m in the West Antarctic Ross and Weddell embayments is much larger than the 150 m found in Gomez et al. (2020), although the spatial pattern of RSL change is similar. The barystatic mean sea level change since LGM we find at 120 m. If we prescribe the present-day AIS configuration through the GIA simulation, we can estimate the far-field RSL pattern in response to northern hemisphere ice sheet loss since LGM. It has a clear imprint of Earth rotational effects, with 75 m in East Antarctica and up to 125 m in West Antarctica (Fig. 10c), and is in agreement with Gomez et al. (2020). Subtracting the far-field RSL pattern provides a first-order estimate of the near-field GIA effects, mainly the deformational and gravitational GIA components. Accordingly, bedrock elevation in the interior of West Antarctica has been uplifted since LGM by up to 540 m, and in East Antarctica by less than 100 m, see Fig. 10d. At the edge of the continental shelf, a peripheral forebulge of opposite sign developed, with up to 85 m vertical bedrock displacement since LGM. This feature is presumably smaller and hence not visible in the corresponding plots of Gomez et al. (2020), likely as a result of the much smaller deglacial AIS losses.

To test the impact of sea level forcing, we have also performed coupled PISM-VILMA simulations with the northern hemisphere ice history fixed at its stage 40 kyr BP, and hence a continuing far-field RSL of around 100 m below its present day value. We found that the AIS remains almost at its LGM state until present day (Fig. S 47) confirming the importance of

sea level in triggering deglacial changes ~~in our simulations,~~ as already stated in Albrecht et al. (2020a). In a similar experiment,
500 Gomez et al. (2020) find a delayed and less pronounced deglacial ~~grounding line~~ GL retreat in Antarctica.
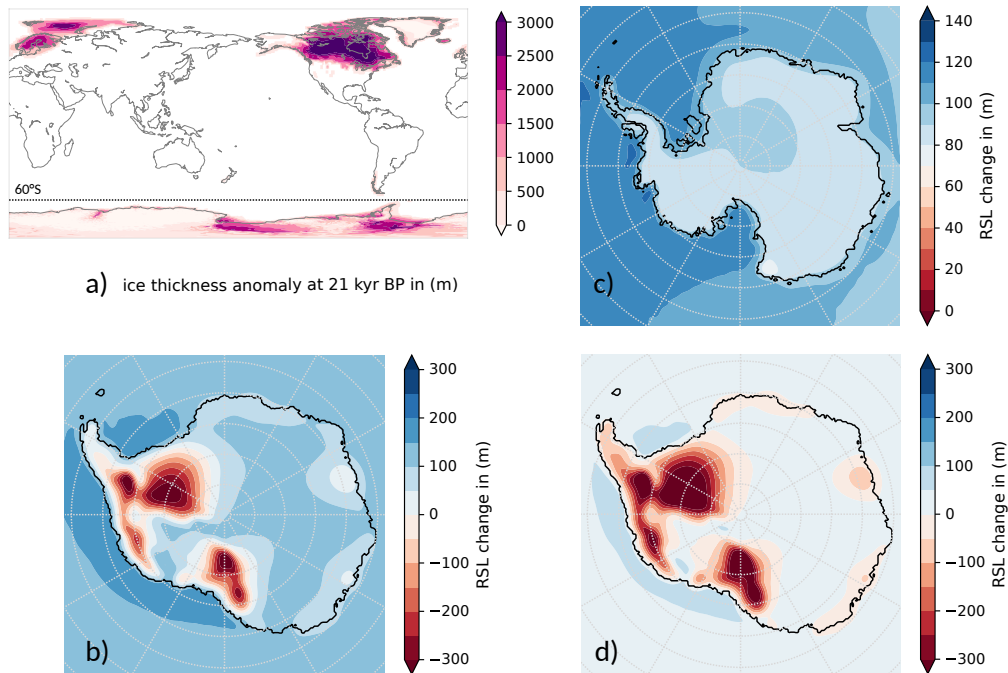
Figure 10. ~~Contributions to deglacial sea level changes in Antarctica, analogous to Gomez et al. (2020)~~ **Far-field and near-field contributions to RSL changes in Antarctica since LGM, analogous to Fig. 1 in Gomez et al. (2020)**

a) ~~Changes in grounded~~ Grounded ice thickness anomaly at 21 kyr BP compared to present day in the coupled PISM-VILMA simulation with ~~reference 3D Earth structure~~ '3D ref' Earth structure, based on the combination of ICE-6G_C ice history in the northern hemisphere (up to the dashed line at 60°S) and the dynamic ice sheet model for Antarctica. b) ~~Associated total relative sea level~~ RSL change since 21 kyr BP in Antarctica. c) Component of ~~relative sea level~~ RSL change associated with ice cover changes in the northern hemisphere, computed from a VILMA simulation with constant present-day ~~Antarctic ice sheet~~ AIS thickness. ~~Note the different color scale.~~ d) Difference between b) and c), ~~showing~~ representing RSL changes ~~in relative sea level~~ associated with Antarctic ice cover changes. These are basically caused by viscoelastic deformation and gravitational effects. Note the difference in color-bar ranges and the values beyond being saturated. The figure design has been chosen similar to Gomez et al. (2020, Fig. 1), to allow a direct comparison.

4   Discussions

A key finding of our coupled ice sheet–solid Earth study is that glacial build-up and deglacial retreat are controlled by different feedbacks, which become dominant for ~~different viscosity regimes that~~ specific viscosity regimes and are associated with ~~different~~ respective response time and length scales (see Sect. 3.2). If the ~~grounding line~~ GL advances, the upstream grounded
505 ice adds additional load. Subsidence and viscoelastically displaced mantle material produces a forebulge ~~in the still ungrounded~~

where ice is still floating, which lowers the water depth and enhances GL advance (see schematic loop Fig. 11a). A weaker Earth structure yields faster and hence deeper subsidence in the interior during ice sheet expansion, as well as a more pronounced forebulge uplift. Figures S 5 illustrates the forebulge evolution near the advancing GL, with height and distance depending on the underlying Earth structure, when considering the first iteration and hence same initial bed elevation.

A thinner elastic lithosphere allows for more localized response, such that the forebulge induced RSL lowering at the GL can offset the RSL rise due to subsidence and gravitational attraction. GL advance supported by forebulge uplift can reach larger glacial ice sheet extents and hence larger ice sheet volumes, which increases loads and induces further subsidence. This is a positive *forebulge feedback* which stops, when the GL reaches the edge of the continental shelf (Fig. 8e, Figs. S 5a–d).

When temperatures rise and the GL starts to retreat into overdeepened embayments, the Marine Ice Sheet Instability (MISI) supports a self-amplified GL retreat. With a thicker cross section, the GL flux increases non-linearly (Schoof, 2007), which reduces the ice thickness there and leads to further retreat (Fig. 11a). Our coupled simulations suggest that a weaker Earth structure causes larger glacial ice sheet extent and more subsidence of the bedrock. This also implies an even steeper retrograde slope (Fig. 11b) and hence an increased potential for MISI-style GL retreat. However, gravitational changes and viscoelastic deformations due to GIA dampen the MISI feedback and slow down the retreat. This stabilizing *sea-level* feedback (e.g. Whitehouse et al., 2019) describes how loss in ice mass leads to lowering in RSL and hence to less GL retreat (see Fig. 11a). In our coupled simulations we did not consider the additional effects related to the Marine Ice Cliff Instability (MICI), whose relevance is under debate at the moment (Lipscomb et al., 2024).

Advancing and retreating GLs during Antarctic glacial cycles pass through roughly the same regions. The largest changes in grounded ice sheet extent (and in RSL) are found in the Weddell Sea and Ross embayments, as well as in the Amundsen and Bellinghausen Sea in West Antarctica, while changes in East Antarctica are comparably small. The weakest Earth structure underneath Antarctica spans between Ross embayment and Amundsen Sea (see Fig. 5). The Earth material becomes stronger towards the Weddell Sea, but is still weaker than the Antarctic-wide logarithmic mean. In the Ross Sea sector the present-day GL position seems loosely constrained by the geometry of the Siple Coast. This region also shows the weakest Earth structure in our setup with a gradual and delayed modeled GL retreat until present day (Neuhaus et al., 2021). We find here the lowest convergence rates in the iterative procedure (Fig. 4), defined as the relative reduction in RMSE between modeled present-day topography and observation in subsequent iterations, which is in line with the findings by Van Calcar et al. (2023).

For GL advance during the glacial build-up, the Earth structure in all those West Antarctic regions seems to be weak enough to be supported by the forebulge feedback. The maximum LGM grounded ice sheet extent from a coupled simulation with the Antarctic-wide minimum of the 3D Earth structure, '3D min', is similar

to '3D ref'. ~~Grounding line~~ GL retreat during deglaciation tends to occur on much shorter time scales ~~then~~ than during glacial build-up. However, due to the ~~GIA~~ sea-level feedback, the retreat can be strongly slowed down in regions with a weak Earth structure, such as in the Ross Sea (Fig. 8). Yet, in the Weddell Sea and Bellinghausen Sea region, the MISI feedback seems to dominate the accelerated ~~grounding line~~ GL retreat. The resultant loss in ~~total (sea level relevant) ice volume~~ SLRP seems to

545 follow a trajectory, which resembles a coupled simulation with the Antarctic-wide maximum or ~~log-mean~~ logarithmic mean of '3D ref', i.e. '3D max' or '3D mean', respectively (see Fig. 7 and Fig. S ~~1~~2). This implies, that in most Antarctic regions '3D ref' is not weak enough to obtain a significant delay of fast deglacial ~~grounding line~~ GL retreat due to the ~~GIA feedback . This~~ sea-level feedback and seems to be a robust feature, as we find a similar response of the ~~Antarctic Ice Sheet~~ AIS for an even larger variability of 3D Earth structures (Fig. S ~~5–7~~8–10).

550 The strength of the solid-Earth structure can be associated with a characteristic response time scale. In our coupled simulations we find a paradoxical behaviour: A weak Earth structure with comparably short response times tends to support ~~the~~ a slow glacial build-up, while it can slow down fast deglacial retreat. As we have a strongly heterogeneous 3D Earth structure, with large differences between East and West Antarctica, but also with moderate differences within West Antarctica, we find a clear asymmetry in the aggregated response to '3D ref': The mantle material is weak enough to support maximum LGM

555 extent, while it is not weak enough to considerably slow down ~~grounding line retreat.~~ GL retreat. When performing iterations over two glacial cycles, this asymmetric response of the coupled system between glacial and deglacial phases requires larger adjustments in initial bed elevation for '3D ref' than for '3D min', which then supports the glacial build-up in the next iteration and leads consequently to larger glacial ice volumes.

5 Conclusions

560 This study presents a new coupling framework between the ice sheet model PISM and the solid Earth model VILMA. We have run coupled simulations over two glacial cycles with PISM for Antarctica and VILMA with a global 3D viscosity structure. ~~We find~~ For coupling time steps of $100\,\mathrm{yr}$ between PISM and VILMA, grid resolutions of $16\,\mathrm{km}$ for PISM in Antarctica, $0.2°$ ($\leq 20\,\mathrm{km}$) for solving the ~~sea level~~ sea-level equation and $0.7°$ ($\leq 78\,\mathrm{km}$) for solving the viscoelastic deformations in VILMA, ~~as sufficient for capturing the~~ we are able to capture relevant dynamics and feedbacks in glacial cycle simulations. We

565 performed an ~~outer iteration scheme~~ iterative correction for initial topography over $246\,\mathrm{kyr}$ (two glacial cycles) to adjust for the ~~weakly constrained~~ initial bed topography. ~~Also, much higher resolutionsare possible for the here applied offline coupling~~ Much higher resolutions, as may be required for an adequate representation of the complex dynamics at the grounding line (GL) in some key regions, can be applied in this offline coupling framework (e.g. $10\,\mathrm{yr}$ coupling time step, order of $1\,\mathrm{km}$ for the ice dynamics and $0.1°$ resolution for the exchange of loading and sea level response); this is possible as the field equations

570 in VILMA are solved in the time-domain, which provides a great flexibility with regard to restart states from which further simulations can be set up.

The tectonic setting of the Antarctic continent reflects strong lateral contrasts in the viscoelastic Earth structure. Our model study highlights the complexity of the interactions between ice sheets, sea level and the solid Earth in Antarctica and world-
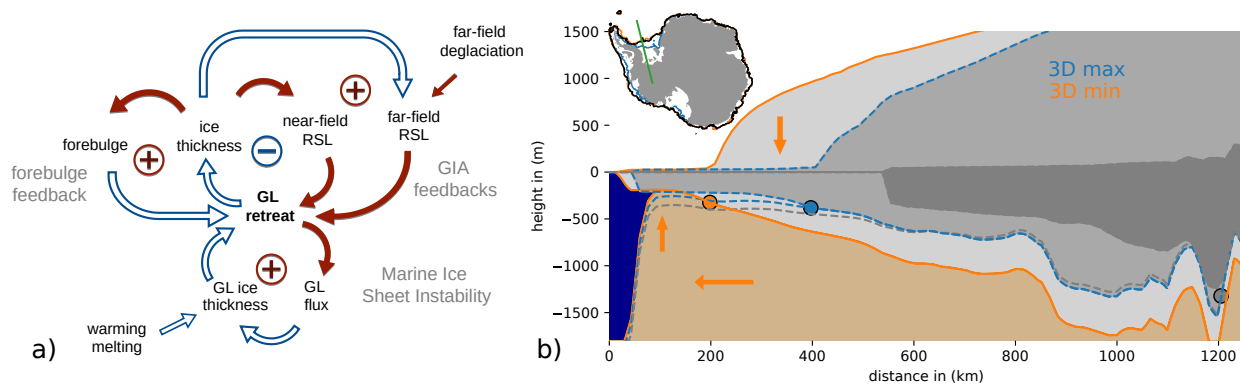
Figure 11. MISI and GIA feedbacks on grounding line migration. a) Feedback loops show the stabilizing near-field ~~of~~ RSL feedback ~~GIA~~ on grounding line (GL) retreat (-) and the self-sustaining forebulge feedback (+) as well as the far-field (barystatic) RSL feedback (+). The Marine Ice Sheet Instability (MISI) represents a self-amplifying ice-internal feedback on ~~grounding line (GL)~~ retreat on retrograde slopes (+), which can be triggered by ocean-induced melting. Amplifying effects are indicated by red filled arrows (e.g. GL retreat leads to more GL flux), dampening effect by non-filled blue arrows (e.g more GL flux results in less ice thickness at the GL). b) Transect shows bedrock elevation and outlines of ice sheet and ice shelf ~~along transect~~ at LGM through Ronne embayment ~~at LGM,~~ from the continental shelf edge to the present-day GL position for the two Antarctic end members of the reference 3D Earth structure, '3D max' and '3D min'. Respective ~~grounding lines locations~~ GL positions (dots) are about 200 km apart. Orange arrows indicate additional ice mass, subsidence of the underlying bedrock, lateral displacement of mantle material and subsequent forebulge uplift. Dark grey shading and dot indicate present-day observed ice sheet configuration and GL position, respectively. Green line in inset indicates transect location.

wide, given the spatial variability and uncertainty of the Earth structure and associated characteristic response-time and length
575 scales. We show that competing feedbacks and time scales are at play during Antarctic glacial build-up and deglaciation.

During phases of glacial build-up, when ~~grounding lines~~ GLs advance over several ten thousands of years, a forebulge can emerge in response to viscoelastic deformations. As the forebulge supports further ~~grounding line~~ GL advance, eventually up to the edge of the continental shelf, it defines a self-amplifying feedback on ice sheet growth - which we phrase as forebulge feedback.

580 In contrast, during deglaciation, ~~grounding line~~ GL retreat can be slowed down as a consequence of the ~~GIA~~ sea-level feedback. In case of a weak Earth structure, it implies ~~,~~ that a fast and localized response of the solid Earth can ~~lead to a slow response of the retreating~~ slow down the retreat rate of the ice sheet. On a retrograde sloping bed topography this stabilizing feedback can counteract the self-amplifying Marine Ice Sheet ~~Instabilty, which favors~~ Instability, the latter favoring fast deglaciation. In case of a stronger Earth structure, and hence longer response time scales, we find rather slow and delayed
585 uplift, which can even cause ~~grounding line~~ GL re-advance, after it has stabilized at topographic features.

Understanding the interplay of feedback mechanisms and involved time scales is highly relevant for the stability analysis of the ~~Antarctic Ice Sheet~~ AIS in a warming climate. In particular, ~~as the grounding lines~~ better constraints on the local Earth structure are required in sensitive key regions of West Antarcica. The GLs of the Amundsen Sea ice shelves (e.g. Pine Island

and Thwaites) are likely entry points for the initialization of the West Antarctic Ice Sheet ~~collapse, possibly also for~~ (WAIS) collapse, and also the stability of the Ross Sea and Weddell Sea ~~. Hence, better constraints on the local Earth structure are required in those particularly sensitive key regions.~~ is under discussion.

Our coupled model system yields self-consistent reconstructions of ice sheet and relative sea level evolutions for 3D solid-Earth structures. The modeled Antarctic ~~ice volume~~ sea-level rise potential at Last Glacial Maximum relative to present-day shows a ~~high sensitivity~~ range between 10 and 15 m SLE for the different considered 3D Earth structures~~we have discussed.~~ ~~This is slightly more~~. These are slightly larger values than in recent coupled ice sheet–solid Earth reconstructions (Gomez et al., 2020; Van Calcar et al., 2023), but within the range of previous model studies (Albrecht et al., 2020b, Fig. 11b). ~~This provides confidence in~~ Based on the gained experience with PISM in high-resolution applications this study adds confidence for the application of the PISM-VILMA coupling framework to future ice sheet ~~and sea level~~ evolution and sea-level projections and the investigation of tipping point characteristics.

Code and data availability. PISM code is freely available and is listed in the Research Software Directory: https://research-software-directory.org/software/pism. VILMA code can be obtained from the authors upon request. The coupling tool is freely available at: https://github.com/talbrecht/pismvilma. The data and processing code will be made publicly available on a public data repository i.e. PANGAEA or Zenodo. DOI links to the repositories will be provided upon publication.

Video supplement. Movie of change rate of relative sea level (RSL) and grounding line dynamics in Antarctica over the last 25 kyr from a coupled ice sheet–solid Earth model system, Copernicus Publications: https://doi.org/10.5446/65479, (Albrecht, 2023), Supplement Video S 1

Supplement.

Author contributions. TA designed the study and developed the coupling framework, with great support by MB and VK. MB provided the 3D viscoelastic Earth structures. TA wrote the manuscript and prepared the figures, with contributions from MB. All authors contributed to the interpretation of model results and revised the manuscript.

Competing interests. The authors declare that they have no competing interests.

Acknowledgements. TA and MB are funded by the German climate modeling project PalMod (FKZ: 01LP1918A, 01LP1925D, 01LP2305A and 01LP2305B) supported by the German Federal Ministry of Education and Research (BMBF) as a Research for Sustainability initia-

tive (FONA). This work also used resources of the German High-Performance Computing Centre for Climate and Earth System Research (DKRZ) granted by its Scientific Steering Committee (WLA) under project ID bk0993. The authors gratefully acknowledge the European Regional Development Fund (ERDF), the German Federal Ministry of Education and Research and the Land Brandenburg for supporting this project by providing resources on the high performance computer system at the Potsdam Institute for Climate Impact Research (PIK). Development of PISM is supported by NASA grants 20-CRYO2020-0052 and 80NSSC22K0274 and NSF grant OAC-2118285. We thank Reyko Schachtschneider for helping revising the manuscript in an early stage.

Review statement. This paper was edited by Alexander Robinson and reviewed by Holly Han and Matt King.

References

A, G., Wahr, J., and Zhong, S.: Computations of the viscoelastic response of a 3-D compressible Earth to surface loading: an application to Glacial Isostatic Adjustment in Antarctica and Canada, Geophysical Journal International, 192, 557–572, https://doi.org/10.1093/gji/ggs030, 2012.

Accardo, N. J., Wiens, D. A., Hernandez, S., Aster, R. C., Nyblade, A., Huerta, A., Anandakrishnan, S., Wilson, T., Heeszel, D. S., and Dalziel, I. W.: Upper mantle seismic anisotropy beneath the West Antarctic Rift System and surrounding region from shear wave splitting analysis, Geophysical Journal International, 198, 414–429, https://doi.org/10.1093/gji/ggu117, 2014.

Adhikari, S., Ivins, E. R., Larour, E., Seroussi, H., Morlighem, M., and Nowicki, S.: Future Antarctic bed topography and its implications for ice sheet dynamics, Solid Earth, 5, 569–584, https://doi.org/10.5194/se-5-569-2014, 2014.

Adhikari, S., Ivins, E. R., Larour, E., Caron, L., and Seroussi, H.: A kinematic formalism for tracking ice–ocean mass exchange on the earth's surface and estimating sea-level change, The Cryosphere, 14, 2819–2833, https://doi.org/10.5194/tc-14-2819-2020, 2020.

Albrecht, T.: Movie: Simulation of the relative sea level change rate around Antarctica with PISM-VILMA over the last 25 kyr, Copernicus Publications, https://doi.org/10.5446/65479, 2023.

Albrecht, T.: PISMVILMA: Coupling of ice sheet model PISM with solid Earth model VILMA, https://github.com/talbrecht/pismvilma, 2024.

Albrecht, T., Winkelmann, R., and Levermann, A.: Glacial-cycle simulations of the Antarctic Ice Sheet with the Parallel Ice Sheet Model (PISM)–Part 1: Boundary conditions and climatic forcing, The Cryosphere, 14, 599–632, https://doi.org/10.5194/tc-14-599-2020, 2020a.

Albrecht, T., Winkelmann, R., and Levermann, A.: Glacial-cycle simulations of the Antarctic Ice Sheet with the Parallel Ice Sheet Model (PISM)–Part 2: Parameter ensemble analysis, The Cryosphere, 14, 633–656, https://doi.org/10.5194/tc-14-633-2020, 2020b.

Amante, C. and Eakins, B. W.: ETOPO1 Arc-Minute Global Relief Model: Procedures, Data Sources and Analysis, NOAA Technical Memorandum NESDIS NGDC-24, National Geophysical Data Center, NOAA, Boulder, https://doi.org/10.7289/V5C8276M, 2009.

An, M., Wiens, D. A., Zhao, Y., Feng, M., Nyblade, A. A., Kanao, M., Li, Y., Maggi, A., and Lévêque, J.-J.: S-velocity model and inferred Moho topography beneath the Antarctic Plate from Rayleigh waves, Journal of Geophysical Research: Solid Earth, 120, 359–383, https://doi.org/10.1002/2014jb011332, 2015.

Armstrong McKay, D. I., Staal, A., Abrams, J. F., Winkelmann, R., Sakschewski, B., Loriani, S., Fetzer, I., Cornell, S. E., Rockström, J., and Lenton, T. M.: Exceeding 1.5 C global warming could trigger multiple climate tipping points, Science, 377, eabn7950, https://doi.org/10.1126/science.abn7950, 2022.

Aschwanden, A. and Blatter, H.: Mathematical modeling and numerical simulation of polythermal glaciers, Journal of Geophysical Research: Earth Surface, 114, https://doi.org/10.1029/2008jf001028, 2009.

Aschwanden, A., Bueler, E., Khroulev, C., and Blatter, H.: An enthalpy formulation for glaciers and ice sheets, Journal of Glaciology, 58, 441–457, https://doi.org/10.3189/2012JoG11J088, 2012.

Bagge, M., Klemann, V., Steinberger, B., Latinović, M., and Thomas, M.: Glacial-Isostatic Adjustment Models Using Geodynamically Constrained 3D Earth Structures, Geochemistry, Geophysics, Geosystems, 22, e2021GC009 853, https://doi.org/10.1029/2021GC009853, 2021.

Bakker, P., Clark, P. U., Golledge, N. R., Schmittner, A., and Weber, M. E.: Centennial-scale Holocene climate variations amplified by Antarctic Ice Sheet discharge, Nature, 541, 72, https://doi.org/10.1038/nature20582, 2017.

Barletta, V. R., Bevis, M., Smith, B. E., Wilson, T., Brown, A., Bordoni, A., Willis, M., Khan, S. A., Rovira-Navarro, M., Dalziel, I., et al.: Observed rapid bedrock uplift in Amundsen Sea Embayment promotes ice-sheet stability, Science, 360, 1335–1339, https://doi.org/10.1126/science.aao1447, 2018.

Behrendt, J. C.: Crustal and lithospheric structure of the West Antarctic Rift System from geophysical investigations—a review, Global and Planetary Change, 23, 25–44, https://doi.org/10.1016/s0921-8181(99)00049-1, 1999.

Blank, B., Barletta, V., Hu, H., Pappa, F., and van der Wal, W.: Effect of Lateral and Stress-Dependent Viscosity Variations on GIA Induced Uplift Rates in the Amundsen Sea Embayment, Geochemistry, Geophysics, Geosystems, 22, e2021GC009 807, https://doi.org/10.1029/2021gc009807, 2021.

Book, C., Hoffman, M. J., Kachuck, S. B., Hillebrand, T. R., Price, S. F., Perego, M., and Bassis, J. N.: Stabilizing effect of bedrock uplift on retreat of Thwaites Glacier, Antarctica, at centennial timescales, Earth and Planetary Science Letters, 597, 117 798, https://doi.org/10.1016/j.epsl.2022.117798, 2022.

Braddock, S., Hall, B. L., Johnson, J. S., Balco, G., Spoth, M., Whitehouse, P. L., Campbell, S., Goehring, B. M., Rood, D. H., and Woodward, J.: Relative sea-level data preclude major late Holocene ice-mass change in Pine Island Bay, Nature Geoscience, pp. 1–5, https://doi.org/10.1038/s41561-022-00961-y, 2022.

Bredow, E., Steinberger, B., Gassmöller, R., and Dannberg, J.: Mantle convection and possible mantle plumes beneath Antarctica – insights from geodynamic models and implications for topography, in: The Geochemistry and Geophysics of the Antarctic Mantle, Geological Society of London, https://doi.org/10.1144/M56-2020-2, 2023.

Briggs, R., Pollard, D., and Tarasov, L.: A glacial systems model configured for large ensemble analysis of Antarctic deglaciation, The Cryosphere, 7, 1949–1970, https://doi.org/10.5194/tc-7-1949-2013, 2013.

Briggs, R. D. and Tarasov, L.: How to evaluate model-derived deglaciation chronologies: a case study using Antarctica, Quaternary Science Reviews, 63, 109–127, https://doi.org/10.1016/j.quascirev.2012.11.021, 2013.

Brotchie, J. F. and Silvester, R.: On crustal flexure, Journal of Geophysical Research, 74, 5240–5252, https://doi.org/10.1029/jb074i022p05240, 1969.

Bueler, E. and Brown, J.: Shallow shelf approximation as a "sliding law" in a thermomechanically coupled ice sheet model, Journal of Geophysical Research: Earth Surface, 114, https://doi.org/10.1029/2008JF001179, 2009.

Bueler, E. and van Pelt, W.: Mass-conserving subglacial hydrology in the Parallel Ice Sheet Model version 0.6, Geoscientific Model Development, 8, 1613, https://doi.org/10.5194/gmd-8-1613-2015, 2015.

Bueler, E., Lingle, C. S., and Brown, J.: Fast computation of a viscoelastic deformable Earth model for ice-sheet simulations, Annals of Glaciology, 46, 97–105, https://doi.org/10.3189/172756407782871567, 2007.

CDO: CDO limate Data Operators, http://mpimet.mpg.de/cdo, accessed 05 June 2024.

Clark, P. U., Dyke, A. S., Shakun, J. D., Carlson, A. E., Clark, J., Wohlfarth, B., Mitrovica, J. X., Hostetler, S. W., and McCabe, A. M.: The Last Glacial Maximum, Science, 325, 710–714, https://doi.org/10.1126/science.1172873, 2009.

Coulon, V., Bulthuis, K., Whitehouse, P. L., Sun, S., Haubner, K., Zipf, L., and Pattyn, F.: Contrasting response of West and East Antarctic ice sheets to glacial isostatic adjustment, Journal of Geophysical Research: Earth Surface, 126, e2020JF006 003, https://doi.org/10.1029/2020jf006003, 2021.

Coulson, S., Lubeck, M., Mitrovica, J. X., Powell, E., Davis, J. L., and Hoggard, M. J.: The Global Fingerprint of Modern Ice-Mass Loss on 3-D Crustal Motion, Geophysical Research Letters, 48, e2021GL095 477, https://doi.org/10.1029/2021gl095477, 2021.

Crawford, A. J., Benn, D. I., Todd, J., Åström, J. A., Bassis, J. N., and Zwinger, T.: Marine ice-cliff instability modeling shows mixed-mode ice-cliff failure and yields calving rate parameterization, Nature communications, 12, 2701, https://doi.org/10.1038/s41467-021-23070-7, 2021.

de Boer, B., Stocchi, P., and Van De Wal, R. S. W.: A fully coupled 3-D ice-sheet–sea-level model: algorithm and applications, Geoscientific Model Development, 7, 2141–2156, https://doi.org/10.5194/gmd-7-2141-2014, 2014.

de Boer, B., Stocchi, P., Whitehouse, P. L., and van de Wal, R. S. W.: Current state and future perspectives on coupled ice-sheet–sea-level modelling, Quaternary Science Reviews, 169, 13–28, https://doi.org/10.1016/j.quascirev.2017.05.013, 2017.

DeConto, R. M. and Pollard, D.: Contribution of Antarctica to past and future sea-level rise, Nature, 531, 591–597, https://doi.org/10.1038/nature17145, 2016.

Dziadek, R., Ferraccioli, F., and Gohl, K.: High geothermal heat flow beneath Thwaites Glacier in West Antarctica inferred from aeromagnetic data, Communications Earth & Environment, 2, 1–6, https://doi.org/10.1038/s43247-021-00242-3, 2021.

Dziewonski, A. M. and Anderson, D. L.: Preliminary reference Earth model, Physics of the earth and planetary interiors, 25, 297–356, https://doi.org/10.1016/0031-9201(81)90046-7, 1981.

Farrell, W. E. and Clark, J. A.: On postglacial sea level, Geophysical Journal International, 46, 647–667, https://doi.org/10.1111/j.1365-246X.1976.tb01252.x, 1976.

Feldmann, J. and Levermann, A.: From cyclic ice streaming to Heinrich-like events: the grow-and-surge instability in the Parallel Ice Sheet Model, The Cryosphere, 11, 1913–1932, https://doi.org/10.5194/tc-11-1913-2017, 2017.

Feldmann, J., Albrecht, T., Khroulev, C., Pattyn, F., and Levermann, A.: Resolution-dependent performance of grounding line motion in a shallow model compared with a full-Stokes model according to the MISMIP3d intercomparison, Journal of Glaciology, 60, 353–360, https://doi.org/10.3189/2014JoG13J093, 2014.

Fretwell, P., Pritchard, H. D., Vaughan, D. G., Bamber, J. L., Barrand, N. E., Bell, R., Bianchi, C., Bingham, R. G., Blankenship, D. D., Casassa, G., Catania, G., Callens, D., Conway, H., Cook, A. J., Corr, H. F. J., Damaske, D., Damm, V., Ferraccioli, F., Forsberg, R., Fujita, S., Gim, Y., Gogineni, P., Griggs, J. A., Hindmarsh, R. C. A., Holmlund, P., Holt, J. W., Jacobel, R. W., Jenkins, A., Jokat, W., Jordan, T., King, E. C., Kohler, J., Krabill, W., Riger-Kusk, M., Langley, K. A., Leitchenkov, G., Leuschen, C., Luyendyk, B. P., Matsuoka, K., Mouginot, J., Nitsche, F. O., Nogi, Y., Nost, O. A., Popov, S. V., Rignot, E., Rippin, D. M., Rivera, A., Roberts, J., Ross, N., Siegert, M. J., Smith, A. M., Steinhage, D., Studinger, M., Sun, B., Tinto, B. K., Welch, B. C., Wilson, D., Young, D. A., Xiangbin, C., and Zirizzotti, A.: Bedmap2: improved ice bed, surface and thickness datasets for Antarctica, The Cryosphere, 7, 375–393, https://doi.org/10.5194/tc-7-375-2013, 2013.

Gladstone, R. M., Payne, A. J., and Cornford, S. L.: Parameterising the grounding line in flow-line ice sheet models, The Cryosphere, 4, 605–619, https://doi.org/10.5194/tc-4-605-2010, 2010.

Goelzer, H., Coulon, V., Pattyn, F., De Boer, B., and Van De Wal, R.: Brief communication: On calculating the sea-level contribution in marine ice-sheet models, The Cryosphere, 14, 833–840, https://doi.org/10.5194/tc-14-833-2020, 2020.

Golledge, N. R., Menviel, L., Carter, L., Fogwill, C. J., England, M. H., Cortese, G., and Levy, R. H.: Antarctic contribution to meltwater pulse 1A from reduced Southern Ocean overturning, Nature communications, 5, 5107, https://doi.org/10.1038/ncomms6107, 2014.

Gomez, N., Mitrovica, J. X., Huybers, P., and Clark, P. U.: Sea level as a stabilizing factor for marine-ice-sheet grounding lines, Nature Geoscience, 3, 850–853, https://doi.org/10.1038/ngeo1012, 2010.

Gomez, N., Pollard, D., Mitrovica, J. X., Huybers, P., and Clark, P. U.: Evolution of a coupled marine ice sheet–sea level model, Journal of Geophysical Research: Earth Surface, 117, https://doi.org/10.1029/2011JF002128, 2012.

Gomez, N., Pollard, D., and Mitrovica, J. X.: A 3-D coupled ice sheet–sea level model applied to Antarctica through the last 40 ky, Earth and Planetary Science Letters, 384, 88–99, https://doi.org/10.1016/j.epsl.2013.09.042, 2013.

Gomez, N., Pollard, D., and Holland, D.: Sea-level feedback lowers projections of future Antarctic Ice-Sheet mass loss, Nature communications, 6, 8798, https://doi.org/10.1038/ncomms9798, 2015.

735 Gomez, N., Latychev, K., and Pollard, D.: A coupled ice sheet–sea level model incorporating 3D earth structure: variations in Antarctica during the last deglacial retreat, Journal of Climate, 31, 4041–4054, https://doi.org/10.1175/JCLI-D-17-0352.1, 2018.

Gomez, N., Weber, M. E., Clark, P. U., Mitrovica, J. X., and Han, H. K.: Antarctic ice dynamics amplified by Northern Hemisphere sea-level forcing, Nature, 587, 600–604, https://doi.org/10.1038/s41586-020-2916-2, 2020.

Gregory, J. M., Griffies, S. M., Hughes, C. W., Lowe, J. A., Church, J. A., Fukimori, I., Gomez, N., Kopp, R. E., Landerer, F., Cozannet,
740 G. L., Ponte, R. M., Stammer, D., Tamisiea, M. E., and van de Wal, R. S. W.: Concepts and Terminology for Sea Level: Mean, Variability and Change, Both Local and Global, Surveys in Geophysics, 40, 1251–1289, https://doi.org/10.1007/s10712-019-09525-z, 2019.

Gudmundsson, G. H.: Ice-shelf buttressing and the stability of marine ice sheets, The Cryosphere, 7, 647–655, https://doi.org/10.5194/tc-7-647-2013, 2013.

Hagedoorn, J. M., Wolf, D., and Martinec, Z.: An estimate of global mean sea-level rise inferred from tide-gauge measurements using glacial-
745 isostatic models consistent with the relative sea-level record, Pure and Applied Geophysics, 164, 791–818, https://doi.org/10.1007/s00024-007-0186-7, 2007.

Han, H. K., Gomez, N., Pollard, D., and DeConto, R.: Modeling Northern Hemispheric Ice Sheet Dynamics, Sea Level Change, and Solid Earth Deformation Through the Last Glacial Cycle, Journal of Geophysical Research: Earth Surface, 126, e2020JF006 040, https://doi.org/10.1029/2020JF006040, 2021.

750 Han, H. K., Gomez, N., and Wan, J. X. W.: Capturing the interactions between ice sheets, sea level and the solid Earth on a range of timescales: a new "time window" algorithm, Geoscientific Model Development, 15, 1355–1373, https://doi.org/10.5194/gmd-15-1355-2022, 2022.

Haseloff, M. and Sergienko, O. V.: The effect of buttressing on grounding line dynamics, Journal of Glaciology, 64, 417–431, https://doi.org/10.1017/jog.2018.30, 2018.

Heeszel, D. S., Wiens, D. A., Anandakrishnan, S., Aster, R. C., Dalziel, I. W., Huerta, A. D., Nyblade, A. A., Wilson, T. J., and Winberry,
755 J. P.: Upper mantle structure of central and West Antarctica from array analysis of Rayleigh wave phase velocities, Journal of Geophysical Research: Solid Earth, 121, 1758–1775, https://doi.org/10.1002/2015jb012616, 2016.

Hewitt, I. and Bradley, A.: Tipping point behaviour of submarine melting in ice-sheet grounding zones, Preprint at Research Square, https://doi.org/10.21203/rs.3.rs-2924707/v1, 2023.

Hindmarsh, R. C. A.: A numerical comparison of approximations to the Stokes equations used in ice sheet and glacier modeling, Journal of
760 Geophysical Research: Earth Surface, 109, https://doi.org/10.1029/2003jf000065, 2004.

Huang, P., Steffen, R., Steffen, H., Klemann, V., Wu, P., van der Wal, W., Martinec, Z., and Tanaka, Y.: A commercial finite element approach to modelling Glacial Isostatic Adjustment on spherical self-gravitating compressible earth models, Geophysical Journal International, 235, 2231–2256, https://doi.org/10.1093/gji/ggad354, 2023.

IPCC: Summary for Policymakers, in: Climate Change 2021: The Physical Science Basis. Contribution of Working Group I to the Sixth
765 Assessment Report of the Intergovernmental Panel on Climate Change, edited by Masson-Delmotte, V., Zhai, P., Pirani, A., Connors, S. L., Péan, C., Berger, S., Caud, N., Chen, Y., Goldfarb, L., Gomis, M. I., Huang, M., Leitzell, K., Lonnoy, E., Matthews, J. B. R., Maycock, T. K., Waterfield, T., Yelekçi, O., Yu, R., and Zhou, B., pp. 3–32, Cambridge University Press, Cambridge, United Kingdom and New York, NY, USA, https://www.ipcc.ch/report/ar6/wg1/downloads/report/IPCC_AR6_WGI_SPM.pdf, 2021.

Ivins, E. R., van der Wal, W., Wiens, D. A., Lloyd, A. J., and Caron, L.: Antarctic upper mantle rheology, in: The Geochemistry and Geophysics of the Antarctic Mantle, edited by Martin, A. P. and van der Wal, W., pp. 267–294, Geological Society of London, https://doi.org/10.1144/M56-2020-19, 2023.

Johnson, J. S., Venturelli, R. A., Balco, G., Allen, C. S., Braddock, S., Campbell, S., Goehring, B. M., Hall, B. L., Neff, P. D., Nichols, K. A., et al.: Existing and potential evidence for Holocene grounding line retreat and readvance in Antarctica, The Cryosphere, 16, 1543–1562, https://doi.org/10.5194/tc-16-1543-2022, 2022.

Jones, R. S., Johnson, J. S., Lin, Y., Mackintosh, A. N., Sefton, J. P., Smith, J. A., Thomas, E. R., and Whitehouse, P. L.: Stability of the Antarctic Ice Sheet during the pre-industrial Holocene, Nature Reviews Earth & Environment, 3, 500–515, https://doi.org/10.1038/s43017-022-00309-5, 2022.

Joughin, I. and Alley, R. B.: Stability of the West Antarctic ice sheet in a warming world, Nature Geoscience, 4, 506–513, https://doi.org/10.1038/ngeo1194, 2011.

Joughin, I., Smith, B. E., and Medley, B.: Marine Ice Sheet Collapse Potentially Underway for the Thwaites Glacier Basin, West Antarctica, Science, 12, 49 055, https://doi.org/10.1126/science.1249055, 2014.

Kendall, R. A., Mitrovica, J. X., and Milne, G. A.: On post-glacial sea level–II. Numerical formulation and comparative results on spherically symmetric models, Geophysical Journal International, 161, 679–706, https://doi.org/10.1111/j.1365-246X.2005.02553.x, 2005.

Kendall, R. A., Latychev, K., Mitrovica, J. X., Davis, J. E., and Tamisiea, M. E.: Decontaminating tide gauge records for the influence of glacial isostatic adjustment: The potential impact of 3-D Earth structure, Geophysical Research Letters, 33, https://doi.org/10.1029/2006GL028448, 2006.

Kingslake, J., Scherer, R. P., Albrecht, T., Coenen, J., Powell, R. D., Reese, R., Stansell, N. D., Tulaczyk, S., Wearing, M. G., and Whitehouse, P. L.: Extensive retreat and re-advance of the West Antarctic ice sheet during the Holocene, Nature, 558, 430, https://doi.org/10.1038/s41586-018-0208-x, 2018.

Klemann, V., Martinec, Z., and Ivins, E. R.: Glacial isostasy and plate motion, Journal of Geodynamics, 46, 95–103, https://doi.org/10.1016/j.jog.2008.04.005, 2008.

Konrad, H., Thoma, M., Sasgen, I., Klemann, V., Grosfeld, K., Barbi, D., and Martinec, Z.: The deformational response of a viscoelastic solid earth model coupled to a thermomechanical ice sheet model, Surveys in Geophysics, 35, 1441–1458, https://doi.org/10.1007/s10712-013-9257-8, 2014.

Konrad, H., Sasgen, I., Pollard, D., and Klemann, V.: Potential of the solid-Earth response for limiting long-term West Antarctic Ice Sheet retreat in a warming climate, Earth and Planetary Science Letters, 432, 254–264, https://doi.org/10.1016/j.epsl.2015.10.008, 2015.

Kreuzer, M., Reese, R., Huiskamp, W. N., Petri, S., Albrecht, T., Feulner, G., and Winkelmann, R.: Coupling framework (1.0) for the PISM (1.1. 4) ice sheet model and the MOM5 (5.1. 0) ocean model via the PICO ice shelf cavity model in an Antarctic domain, Geoscientific Model Development, 14, 3697–3714, https://doi.org/10.5194/gmd-14-3697-2021, 2021.

Larour, E., Seroussi, H., Adhikari, S., Ivins, E., Caron, L., Morlighem, M., and Schlegel, N.: Slowdown in Antarctic mass loss from solid Earth and sea-level feedbacks, Science, 364, eaav7908, https://doi.org/0.1126/science.aav7908, 2019.

Latychev, K., Mitrovica, J. X., Tromp, J., Tamisiea, M. E., Komatitsch, D., and Christara, C. C.: Glacial isostatic adjustment on 3-D Earth models: a finite-volume formulation, Geophysical Journal International, 161, 421–444, https://doi.org/10.1111/j.1365-246x.2005.02536.x, 2005.

Le Meur, E. and Huybrechts, P.: A comparison of different ways of dealing with isostasy: examples from modelling the Antarctic ice sheet during the last glacial cycle, Annals of Glaciology, 23, 309–317, https://doi.org/10.1017/s0260305500013586, 1996.

Lenton, T. M., Armstrong McKay, D. I., Loriani, S., Abrams, J., Lade, S., Donges, J., Milkoreit, M., Powell, T., Smith, S., Zimm, C., Buxton, J., Bailey, E., Laybourn, L., Ghadiali, A., and Dyke (eds), J.: The Global Tipping Points Report 2023, Tech. rep., University of Exeter, Exeter, UK, https://global-tipping-points.org, 2023.

810   Levermann, A., Albrecht, T., Winkelmann, R., Martin, M., Haseloff, M., and Joughin, I.: Kinematic first-order calving law implies potential for abrupt ice-shelf retreat, The Cryosphere, 6, 273–286, https://doi.org/10.5194/tc-6-273-2012, 2012.

Li, D.: Physical processes and feedbacks obscuring the future of the Antarctic Ice Sheet, Geosystems and Geoenvironment, 1, 100 084, https://doi.org/j.geogeo.2022.100084, 2022.

Lingle, C. S. and Clark, J. A.: A numerical model of interactions between a marine ice sheet and the solid earth: Application to a West

815   Antarctic ice stream, Journal of Geophysical Research: Oceans, 90, 1100–1114, https://doi.org/10.1029/jc090ic01p01100, 1985.

Lipscomb, W. H., Behar, D., and Morrison, M. A.: Brief communication: Sea-level projections, adaptation planning, and actionable science, EGUsphere, 2024, 1–14, https://doi.org/10.5194/egusphere-2024-534, 2024.

Lliboutry, L. and Duval, P.: Various isotropic and anisotropic ices found in glaciers and polar ice caps and their corresponding rheologies: Ann Geophys V3, N2, March–April 1985, P207–224, International Journal of Rock Mechanics and Mining Sciences & Geomechanics

820   Abstracts, 22, 198, https://doi.org/https://doi.org/10.1016/0148-9062(85)90267-0, 1985.

Lloyd, A. J., Wiens, D. A., Zhu, H., Tromp, J., Nyblade, A. A., Aster, R. C., Hansen, S. E., Dalziel, I. W., Wilson, T. J., Ivins, E. R., et al.: Seismic structure of the Antarctic upper mantle imaged with adjoint tomography, Journal of Geophysical Research: Solid Earth, 125, https://doi.org/10.1029/2019JB017823, 2020.

Lough, A. C., Wiens, D. A., Grace Barcheck, C., Anandakrishnan, S., Aster, R. C., Blankenship, D. D., Huerta, A. D., Nyblade, A., Young,

825   D. A., and Wilson, T. J.: Seismic detection of an active subglacial magmatic complex in Marie Byrd Land, Antarctica, Nature Geoscience, 6, 1031–1035, https://doi.org/10.1038/ngeo1992, 2013.

Lowry, D., Han, H. K., Golledge, N., Gomez, N., Johnson, K., and McKay, R.: Ocean cavity regime shift reversed West Antarctic grounding line retreat in the late Holocene, Nature Communications, 15, 3176, https://doi.org/10.1038/s41467-024-47369-3, 2024.

Maptiler: WGS 84 / Antarctic Polar Stereographic, https://epsg.io/3031, accessed 05 June 2024, 2024.

830   Martinec, Z.: Program to calculate the spectral harmonic expansion coefficients of the two scalar fields product, Computer Physics Communications, 54, 177–182, https://doi.org/10.1016/0010-4655(89)90043-X, 1989.

Martinec, Z.: Spectral–finite element approach to three-dimensional viscoelastic relaxation in a spherical earth, Geophysical Journal International, 142, 117–141, https://doi.org/10.1046/j.1365-246x.2000.00138.x, 2000.

Martinec, Z. and Hagedoorn, J.: The rotational feedback on linear-momentum balance in glacial isostatic adjustment, Geophysical Journal

835   International, 199, 1823–1846, https://doi.org/10.1093/gji/ggu369, 2014.

Martinec, Z., Klemann, V., van der Wal, W., Riva, R. E. M., Spada, G., Sun, Y., Melini, D., Kachuck, S. B., Barletta, V., Simon, K., A, G., and James, T. S.: A benchmark study of numerical implementations of the sea level equation in GIA modelling, Geophysical Journal International, 215, 389–414, https://doi.org/10.1093/gji/ggy280, 2018.

Mercer, J. H.: West Antarctic ice sheet and CO2 greenhouse effect: a threat of disaster, Nature, 271, 321, https://doi.org/10.1038/271321a0,

840   1978.

Milne, G. A. and Mitrovica, J. X.: Postglacial sea-level change on a rotating Earth: first results from a gravitationally self-consistent sea-level equation, Geophysical Journal International, 126, F13–F20, https://doi.org/10.1111/j.1365-246x.1996.tb04691.x, 1996.

Mitrovica, J. and Milne, G.: On the origin of late Holocene sea-level highstands within equatorial ocean basins, Quaternary Science Reviews, 21, 2179–2190, https://doi.org/10.1016/S0277-3791(02)00080-X, 2002.

845   Mitrovica, J. X. and Milne, G. A.: On post-glacial sea level: I. General theory, Geophysical Journal International, 154, 253–267, https://doi.org/10.1046/j.1365-246X.2003.01942.x, 2003.

Mitrovica, J. X. and Peltier, W. R.: On postglacial geoid subsidence over the equatorial oceans, Journal of Geophysical Research: Solid Earth, 96, 20 053–20 071, https://doi.org/10.1029/91JB01284, 1991.

Mitrovica, J. X., Tamisiea, M. E., Davis, J. L., and Milne, G. A.: Recent mass balance of polar ice sheets inferred from patterns of global
850   sea-level change, Nature, 409, 1026–1029, https://doi.org/10.1038/35059054, 2001.

Mitrovica, J. X., Wahr, J., Matsuyama, I., and Paulson, A.: The rotational stability of an ice-age earth, Geophysical Journal International, 161, 491–506, https://doi.org/10.1111/j.1365-246X.2005.02609.x, 2005.

Morelli, A. and Danesi, S.: Seismological imaging of the Antarctic continental lithosphere: a review, Global and Planetary Change, 42, 155–165, https://doi.org/10.1016/j.gloplacha.2003.12.005, 2004.

855   Morlighem, M., Rignot, E., Binder, T., Blankenship, D., Drews, R., Eagles, G., Eisen, O., Ferraccioli, F., Forsberg, R., Fretwell, P., et al.: Deep glacial troughs and stabilizing ridges unveiled beneath the margins of the Antarctic ice sheet, Nature Geoscience, 13, 132–137, https://doi.org/10.1038/s41561-019-0510-8, 2020.

NCO: Command-line operators for netCDF and HDF files, https://nco.sourceforge.net, accessed 05 June 2024, 2003-2024.

Neuhaus, S. U., Tulaczyk, S. M., Stansell, N. D., Coenen, J. J., Scherer, R. P., Mikucki, J. A., and Powell, R. D.: Did Holocene climate
860   changes drive West Antarctic grounding line retreat and readvance?, The Cryosphere, 15, 4655–4673, https://doi.org/10.5194/tc-15-4655-2021, 2021.

Nield, G. A., Barletta, V. R., Bordoni, A., King, M. A., Whitehouse, P. L., Clarke, P. J., Domack, E., Scambos, T. A., and Berthier, E.: Rapid bedrock uplift in the Antarctic Peninsula explained by viscoelastic response to recent ice unloading, Earth and Planetary Science Letters, 397, 32–41, https://doi.org/10.1016/j.epsl.2014.04.019, 2014.

865   Nield, G. A., Whitehouse, P. L., van der Wal, W., Blank, B., O'Donnell, J. P., and Stuart, G. W.: The impact of lateral variations in lithospheric thickness on glacial isostatic adjustment in West Antarctica, Geophysical Journal International, 214, 811–824, https://doi.org/10.1093/gji/ggy158, 2018.

Nowicki, S., Goelzer, H., Seroussi, H., Payne, A. J., Lipscomb, W. H., Abe-Ouchi, A., Agosta, C., Alexander, P., Asay-Davis, X. S., Barthel, A., et al.: Experimental protocol for sea level projections from ISMIP6 stand-alone ice sheet models, The Cryosphere, 14, 2331–2368,
870   https://doi.org/10.5194/tc-14-2331-2020, 2020.

Nowicki, S. M. J., Payne, A., Larour, E., Seroussi, H., Goelzer, H., Lipscomb, W., Gregory, J., Abe-Ouchi, A., and Shepherd, A.: Ice Sheet Model Intercomparison Project (ISMIP6) contribution to CMIP6, Geoscientific Model Development, 9, 4521, https://doi.org/10.5194/gmd-9-4521-2016, 2016.

OpenMP: The OpenMP API specification for parallel programming, https://www.openmp.org/resources/refguides, accessed: 05 June 2024,
875   2012-2023.

Otosaka, I. N., Horwath, M., Mottram, R., and Nowicki, S.: Mass Balances of the Antarctic and Greenland Ice Sheets Monitored from Space, Surveys in Geophysics, 44, 1615–1652, https://doi.org/10.1007/s10712-023-09795-8, 2023.

Pan, L., Powell, E. M., Latychev, K., Mitrovica, J. X., Creveling, J. R., Gomez, N., Hoggard, M. J., and Clark, P. U.: Rapid postglacial rebound amplifies global sea level rise following West Antarctic Ice Sheet collapse, Science Advances, 7, eabf7787,
880   https://doi.org/10.1126/sciadv.abf7787, 2021.

Pattyn, F.: Sea-level response to melting of Antarctic ice shelves on multi-centennial timescales with the fast Elementary Thermomechanical Ice Sheet model (f. ETISh v1. 0), The Cryosphere, 11, 1851–1878, https://doi.org/0.5194/tc-11-1851-2017, 2017.

Pattyn, F. and Morlighem, M.: The uncertain future of the Antarctic Ice Sheet, Science, 367, 1331–1335, https://doi.org/10.1126/science.aaz5487, 2020.

885 Pattyn, F., Perichon, L., Durand, G., Favier, L., Gagliardini, O., Hindmarsh, R. C., Zwinger, T., Albrecht, T., Cornford, S., Docquier, D., et al.: Grounding-line migration in plan-view marine ice-sheet models: results of the ice2sea MISMIP3d intercomparison, Journal of Glaciology, 59, 410–422, https://doi.org/10.3189/2013jog12j129, 2013.

Pegler, S. S.: Marine ice sheet dynamics: the impacts of ice-shelf buttressing, Journal of Fluid Mechanics, 857, 605–647, https://doi.org/10.1017/jfm.2018.741, 2018.

890 Peltier, W.: On the hemispheric origins of meltwater pulse 1a, Quaternary Science Reviews, 24, 1655–1671, https://doi.org/10.1016/j.quascirev.2004.06.023, 2005.

Peltier, W., Argus, D., and Drummond, R.: Space geodesy constrains ice age terminal deglaciation: The global ICE-6G_C (VM5a) model, Journal of Geophysical Research: Solid Earth, 120, 450–487, https://doi.org/10.1002/2014JB011176, 2015.

Peltier, W. R.: The impulse response of a Maxwell Earth, Reviews of Geophysics, 12, 649–669, https://doi.org/10.1029/rg012i004p00649,
895 1974.

PISM User Manual: PISM, a Parallel Ice Sheet Model: User's Manual, https://www.pism.io/docs, based on stable v.2.1 edn., accessed 05 June 2024, 2023.

Pollard, D. and DeConto, R.: Description of a hybrid ice sheet-shelf model, and application to Antarctica, Geoscientific Model Development, 5, 1273–1295, https://doi.org/10.5194/gmd-5-1273-2012, 2012.

900 Pollard, D., DeConto, R. M., and Alley, R. B.: Potential Antarctic Ice Sheet retreat driven by hydrofracturing and ice cliff failure, Earth and Planetary Science Letters, 412, 112–121, https://doi.org/10.1016/j.epsl.2014.12.035, 2015.

Pollard, D., Gomez, N., and Deconto, R. M.: Variations of the Antarctic Ice Sheet in a Coupled Ice Sheet-Earth-Sea Level Model: Sensitivity to Viscoelastic Earth Properties, Journal of Geophysical Research: Earth Surface, 122, 2124–2138, https://doi.org/10.1002/2017JF004371, 2017.

905 Powell, E., Gomez, N., Hay, C., Latychev, K., and Mitrovica, J.: Viscous effects in the solid Earth response to modern Antarctic ice mass flux: Implications for geodetic studies of WAIS stability in a warming world, Journal of Climate, 33, 443–459, https://doi.org/10.1175/jcli-d-19-0479.1, 2020.

Powell, E. M., Pan, L., Hoggard, M. J., Latychev, K., Gomez, N., Austermann, J., and Mitrovica, J. X.: The impact of 3-D Earth structure on far-field sea level following interglacial West Antarctic Ice Sheet collapse, Quaternary Science Reviews, 273, 107 256,
910 https://doi.org/10.1016/j.quascirev.2021.107256, 2021.

Quiquet, A., Dumas, C., Ritz, C., Peyaud, V., and Roche, D. M.: The GRISLI ice sheet model (version 2.0): calibration and validation for multi-millennial changes of the Antarctic ice sheet, Geoscientific Model Development, 11, 5003–5025, https://doi.org/10.5194/gmd-11-5003-2018, 2018.

Ramirez, C., Nyblade, A., Hansen, S., Wiens, D. A., Anandakrishnan, S., Aster, R. C., Huerta, A. D., Shore, P., and Wilson, T.: Crustal
915 and upper-mantle structure beneath ice-covered regions in Antarctica from S-wave receiver functions and implications for heat flow, Geophysical Journal International, 204, 1636–1648, https://doi.org/10.1093/gji/ggv542, 2016.

Reed, B., Green, J., Jenkins, A., and Gudmundsson, G. H.: Recent irreversible retreat phase of Pine Island Glacier, Nature Climate Change, https://doi.org/10.1038/s41558-023-01887-y, 2023.

Reese, R., Albrecht, T., Mengel, M., Asay-Davis, X., and Winkelmann, R.: Antarctic sub-shelf melt rates via PICO, The Cryosphere, 12,
920 1969, https://doi.org/10.5194/tc-12-1969-2018, 2018a.

Reese, R., Gudmundsson, G. H., Levermann, A., and Winkelmann, R.: The far reach of ice-shelf thinning in Antarctica, Nature Climate Change, 8, 53–57, https://doi.org/10.1038/s41558-017-0020-x, 2018b.

Reese, R., Winkelmann, R., and Gudmundsson, G. H.: Grounding-line flux formula applied as a flux condition in numerical simulations fails for buttressed Antarctic ice streams, The Cryosphere, 12, 3229–3242, https://doi.org/10.5194/tc-12-3229-2018, 2018c.

925 Rignot, E., Mouginot, J., Morlighem, M., Seroussi, H., and Scheuchl, B.: Widespread, rapid grounding line retreat of Pine Island, Thwaites, Smith, and Kohler glaciers, West Antarctica, from 1992 to 2011, Geophysical Research Letters, 41, 3502–3509, https://doi.org/10.1002/2014GL060140, 2014.

Rignot, E., Mouginot, J., Scheuchl, B., Van Den Broeke, M., Van Wessem, M. J., and Morlighem, M.: Four decades of Antarctic Ice Sheet mass balance from 1979–2017, Proceedings of the National Academy of Sciences, 116, 1095–1103,
930 https://doi.org/10.1073/pnas.1812883116, 2019.

Schannwell, C., Mikolajewicz, U., Ziemen, F., and Kapsch, M.-L.: Sensitivity of Heinrich-type ice-sheet surge characteristics to boundary forcing perturbations, Climate of the Past, 19, 179–198, https://doi.org/10.5194/cp-19-179-2023, 2023.

Schoof, C.: Ice sheet grounding line dynamics: Steady states, stability, and hysteresis, Journal of Geophysical Research, 112, https://doi.org/10.1029/2006JF000664, 2007.

935 Seroussi, H. and Morlighem, M.: Representation of basal melting at the grounding line in ice flow models, The Cryosphere, 12, 3085–3096, https://doi.org/10.5194/tc-12-3085-2018, 2018.

Seroussi, H., Nowicki, S., Payne, A. J., Goelzer, H., Lipscomb, W. H., Abe-Ouchi, A., Agosta, C., Albrecht, T., Asay-Davis, X., Barthel, A., et al.: ISMIP6 Antarctica: a multi-model ensemble of the Antarctic ice sheet evolution over the 21st century, The Cryosphere, 14, 3033–3070, https://doi.org/10.5194/egusphere-egu2020-6309, 2020.

940 SLURM: SLURM workload manager, https://slurm.schedmd.com/, 2003-2024.

Spada, G., Barletta, V. R., Klemann, V., Riva, R. E. M., Martinec, Z., Gasperini, P., Lund, B., Wolf, D., Vermeersen, L. L. A., and King, M. A.: A benchmark study for glacial isostatic adjustment codes, Geophysical Journal International, 185, 106–132, https://doi.org/10.1111/j.1365-246X.2011.04952.x, 2011.

Spada, G., Bamber, J. L., and Hurkmans, R. T. W. L.: The gravitationally consistent sea-level fingerprint of future terrestrial ice loss,
945 Geophysical Research Letters, 40, 482–486, https://doi.org/10.1029/2012gl053000, 2013.

Steinberger, B.: Topography caused by mantle density variations: observation-based estimates and models derived from tomography and lithosphere thickness, Geophysical Journal International, 205, 604–621, https://doi.org/10.1093/gji/ggw040, 2016.

Stocchi, P., Escutia, C., Houben, A. J., Vermeersen, B. L., Bijl, P. K., Brinkhuis, H., DeConto, R. M., Galeotti, S., Passchier, S., Pollard, D., et al.: Relative sea-level rise around East Antarctica during Oligocene glaciation, Nature Geoscience, 6, 380–384,
950 https://doi.org/10.1038/ngeo1783, 2013.

Sutter, J., Fischer, H., Grosfeld, K., Karlsson, N. B., Kleiner, T., Van Liefferinge, B., and Eisen, O.: Modelling the Antarctic Ice Sheet across the mid-Pleistocene transition – implications for Oldest Ice, The Cryosphere, 13, 2023–2041, https://doi.org/10.5194/tc-13-2023-2019, 2019.

Swierczek-Jereczek, J., Montoya, M., Latychev, K., Robinson, A., Alvarez-Solas, J., and Mitrovica, J.: FastIsostasy v1.0 – An accelerated
955 regional GIA model accounting for the lateral variability of the solid Earth, EGUsphere, 2023, 1–34, https://doi.org/10.5194/egusphere-2023-2869, 2023.

The PISM authors: Parallel Ice Sheet Model (PISM), https://doi.org/10.5281/ZENODO.10202029, accessed 05 June 2024, 2023.

Thomas, R. H. and Bentley, C. R.: A model for Holocene retreat of the West Antarctic ice sheet, Quaternary Research, 10, 150–170, https://doi.org/10.1016/0033-5894(78)90098-4, 1978.

960 Van Calcar, C. J., Van De Wal, R. S., Blank, B., De Boer, B., and Van Der Wal, W.: Simulation of a fully coupled 3D glacial iso-
static adjustment–ice sheet model for the Antarctic ice sheet over a glacial cycle, Geoscientific Model Development, 16, 5473–5492,
https://doi.org/10.5194/gmd-16-5473-2023, 2023.

Van den Berg, J., Van de Wal, R., Milne, G., and Oerlemans, J.: Effect of isostasy on dynamical ice sheet modeling: A case study for Eurasia,
Journal of Geophysical Research: Solid Earth, 113, https://doi.org/10.1029/2007JB004994, 2008.

965 van der Wal, W., Whitehouse, P. L., and Schrama, E. J.: Effect of GIA models with 3D composite mantle viscosity on GRACE mass balance
estimates for Antarctica, Earth and Planetary Science Letters, 414, 134–143, https://doi.org/10.1016/j.epsl.2015.01.001, 2015.

Wan, J. X. W., Gomez, N., Latychev, K., and Han, H. K.: Resolving glacial isostatic adjustment (GIA) in response to modern and future ice
loss at marine grounding lines in West Antarctica, The Cryosphere, 16, 2203–2223, https://doi.org/10.5194/tc-16-2203-2022, 2022.

Weber, M. E., Clark, P. U., Kuhn, G., Timmermann, A., Sprenk, D., Gladstone, R., Zhang, X., Lohmann, G., Menviel, L., Chikamoto,
970 M. O., Friedrich, T., and Ohlwein, C.: Millennial-scale variability in Antarctic ice-sheet discharge during the last deglaciation, Nature,
510, 134–138, https://doi.org/10.1038/nature13397, 00002, 2014.

Weertman, J.: Stability of the junction of an ice sheet and an ice shelf, Journal of Glaciology, 13, 3–11,
https://doi.org/10.1017/s0022143000023327, 1974.

Whitehouse, P. L.: Glacial isostatic adjustment modelling: historical perspectives, recent advances, and future directions, Earth Surface
975 Dynamics, 6, 401–429, https://doi.org/10.5194/esurf-6-401-2018, 2018.

Whitehouse, P. L., Bentley, M. J., Milne, G. A., King, M. A., and Thomas, I. D.: A new glacial isostatic adjustment model for Antarctica:
calibrated and tested using observations of relative sea-level change and present-day uplift rates, Geophysical Journal International, 190,
1464–1482, https://doi.org/10.1111/j.1365-246X.2012.05557.x, 2012.

Whitehouse, P. L., Gomez, N., King, M. A., and Wiens, D. A.: Solid Earth change and the evolution of the Antarctic Ice Sheet, Nature
980 communications, 10, 503, https://doi.org/10.1038/s41467-018-08068-y, 2019.

Willeit, M., Ganopolski, A., Robinson, A., and Edwards, N. R.: The Earth system model CLIMBER-X v1.0 – Part 1: climate model descrip-
tion and validation, Geoscientific Model Development, 15, 5905–5948, https://doi.org/10.5194/gmd-15-5905-2022, 2022.

Winkelmann, R., Martin, M. A., Haseloff, M., Albrecht, T., Bueler, E., Khroulev, C., and Levermann, A.: The Potsdam Parallel Ice Sheet
Model (PISM-PIK) – Part 1: Model description, The Cryosphere, 5, 715–726, https://doi.org/10.5194/tc-5-715-2011, 2011.

985 Wu, P., Wang, H., and Schotman, H.: Postglacial induced surface motions, sea-levels and geoid rates on a spherical, self-gravitating laterally
heterogeneous earth, Journal of Geodynamics, 39, 127–142, https://doi.org/10.1016/j.jog.2004.08.006, 2005.

Yang, H., Krebs-Kanzow, U., Kleiner, T., Sidorenko, D., Rodehacke, C. B., Shi, X., Gierz, P., Niu, L., Gowan, E. J., Hinck,
S., et al.: Impact of paleoclimate on present and future evolution of the Greenland Ice Sheet, Plos one, 17, e0259816,
https://doi.org/10.1371/journal.pone.0259816, 2022.

990 Yousefi, M., Wan, J., Pan, L., Gomez, N., Latychev, K., Mitrovica, J., Pollard, D., and DeConto, R.: The Influence of the Solid Earth
on the Contribution of Marine Sections of the Antarctic Ice Sheet to Future Sea-Level Change, Geophysical Research Letters, 49,
e2021GL097525, https://doi.org/10.1029/2021GL097525, 2022.

Zeitz, M., Haacker, J. M., Donges, J. F., Albrecht, T., and Winkelmann, R.: Dynamic regimes of the Greenland Ice Sheet emerging from in-
teracting melt–elevation and glacial isostatic adjustment feedbacks, Earth System Dynamics, 13, 1077–1096, https://doi.org/10.5194/esd-
995 13-1077-2022, 2022.

Zhong, S., Kang, K., A, G., and Qin, C.: CitcomSVE: A Three-Dimensional Finite Element Software Package for Modeling Planetary Mantle's Viscoelastic Deformation in Response to Surface and Tidal Loads, Geochemistry, Geophysics, Geosystems, 23, https://doi.org/10.1029/2022gc010359, 2022.

Ziemen, F. A., Kapsch, M.-L., Klockmann, M., and Mikolajewicz, U.: Heinrich events show two-stage climate response in transient glacial simulations, Climate of the Past, 15, 153–168, https://doi.org/10.5194/cp-15-153-2019, 2019.

Zwally, H. J., Giovinetto, M. B., Beckley, M. A., and Saba, J. L.: Antarctic and Greenland drainage systems, GSFC cryospheric sciences laboratory, http://imbie.org/imbie-2016/drainage-basins/, 2012.

1000

Supplement to manuscript:

Feedback mechanisms controlling Antarctic glacial cycle dynamics simulated with a coupled ice sheet–solid Earth model

Torsten Albrecht [1], Meike Bagge [2, 3], and Volker Klemann [2]

[1]Potsdam Institute for Climate Impact Research (PIK), Member of the Leibniz Association, Potsdam, Germany
[2]Helmholtz Centre Potsdam, German Research Centre for Geosciences - GFZ, Potsdam, Germany
[3]now at: Federal Institute for Geosciences and Natural Resources, Hanover, Germany

Correspondence: T. Albrecht (albrecht@pik-potsdam.de)

In this supplement, we present further material. It is used in the manuscript to stress the discussed results. In addition (p. 8ff.), we show the impact of further 3D structures, which are based on the investigation of Bagge et al. (2021) and which highlights the sensitivity of Antarctic Ice Sheet response to spatial variability in 3D Earth structures.

List of supplementary figures

List of supplementary videos

Figure S 1. Difference in RSL between different spatial resolutions at 10 kyr BP in West Antarctica. Black is the GL for the reference resolution n512, colored are the GL for resolution of n64, n128, n256 and n1024, respectively.

Sea-level relevant Antarctic ice volume and grounded ice area over last 20 kyr for different Earth structure configurations.
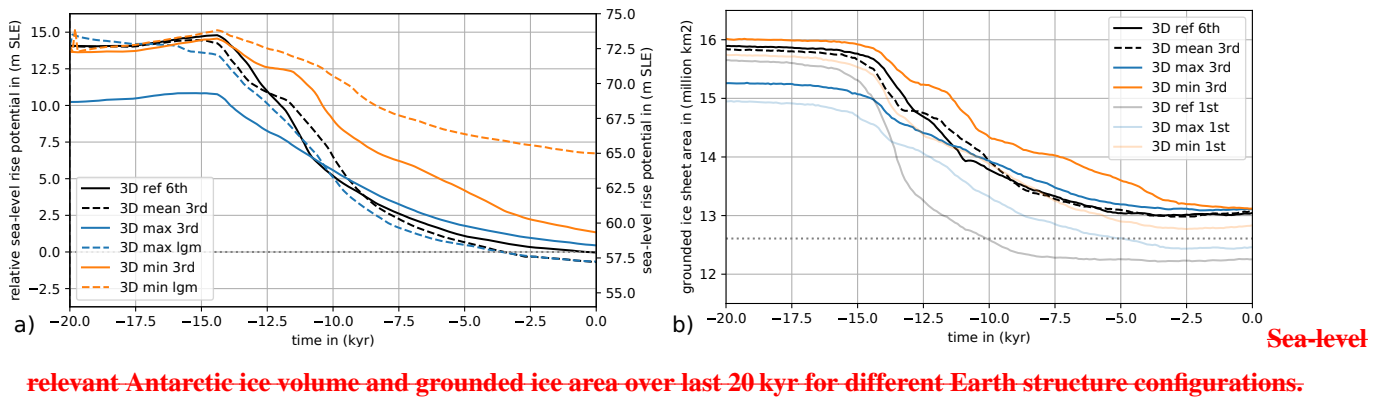
Figure S 2. Sea-level rise potential and grounded ice sheet area over last 20 kyr for different Earth structure configurations. a) Sea-level ~~relevant Antarctic ice volume~~ rise potential in last iteration relative to present-day observations for '3D ref', '3D max' and '3D min' as well as the ice sheet's response for '3D max' and '3D min', when spun-up with the ice ~~volume~~ load history of the '3D ref' case until 20 kyr BP ('lgm'). Black dashed is the ice sheet response for '3D mean'. b) Grounded ice sheet area in three cases, with transparent lines for first iteration. Dotted horizontal line ~~is~~ represents the present-day observation from Bedmap2 (Fretwell et al., 2013), .
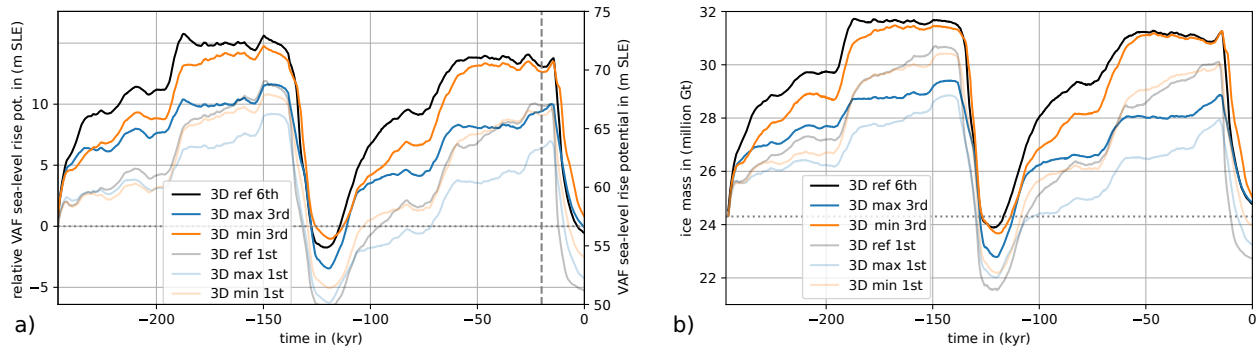
Figure S3. **Antarctic ice volume above flotation and total ice mass over last 246 kyr for different Earth structure configurations.** a) Sea-level rise potential from Antarctica in first and last iteration for '3D ref', '3D max' and '3D min' without the corrections applied according to Adhikari et al. (2020). The calculation of the 'volume above flotation' (VAF) follows Eq. 2 in (Goelzer et al., 2020, see Corrigendum). b) Total ice mass in the three cases, with transparent lines for first iteration. Dotted horizontal line represents the present-day observation from Bedmap2 (Fretwell et al., 2013). Initial ice masses are all identical.
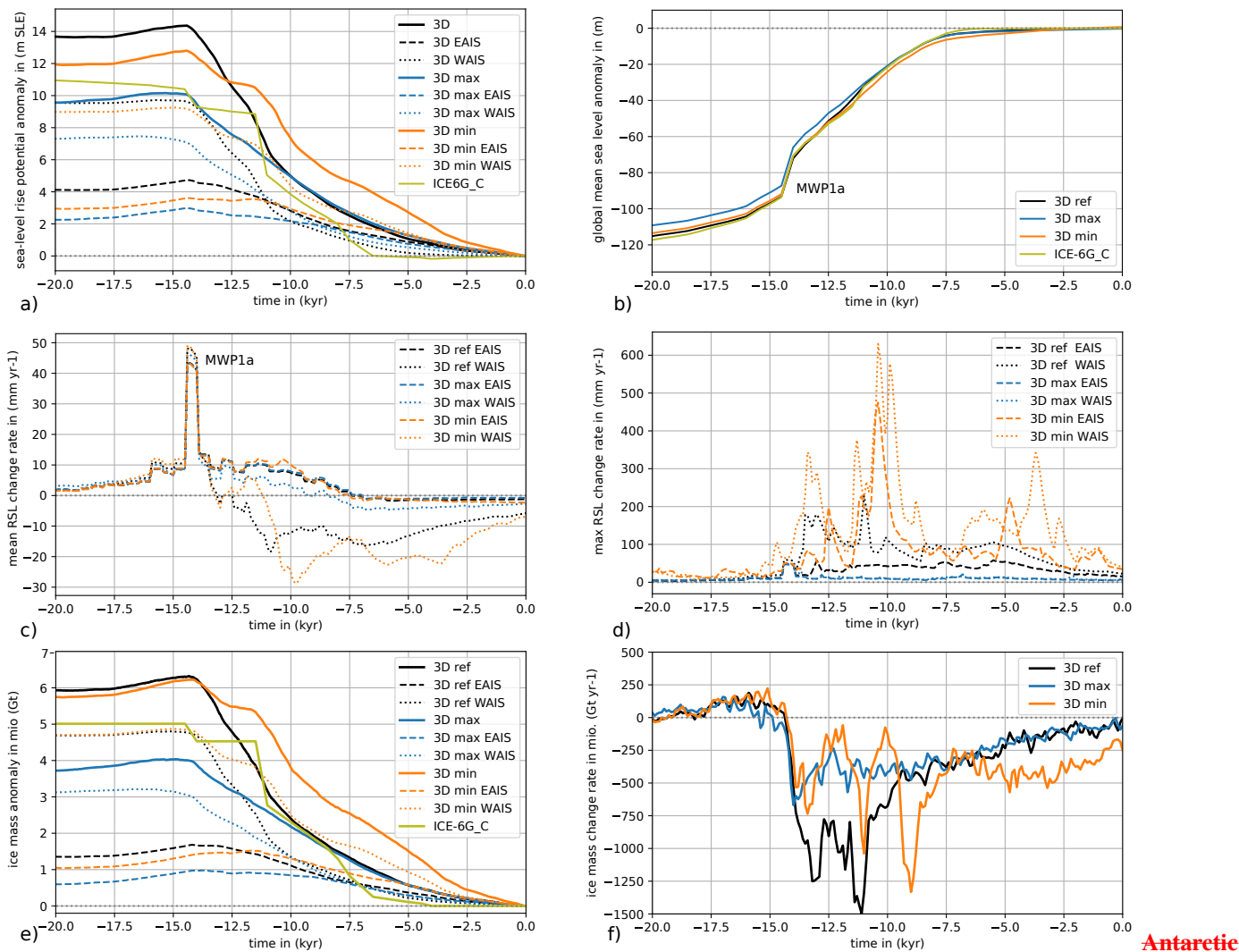
Antarctic ice volume and change in relative sea level over last 20 kyr for different Earth structures.

Figure S 4. ~~Anomalies and change rates in sea level metrics over last 20 kyr for different Earth structures.~~ a) Anomaly in ~~sea-level relevant Antarctic ice volume~~SLRP in Antarctica, b) global mean change in relative sea level (RSL), c) mean change rates of RSL, d) maximum change rates of RSL, e) anomaly in Antarctic ice mass and f) change rates in Antarctic ice mass with 100 yr resolution. Blue and orange lines show the response of the ice sheet to '3D max' and '3D min' Earth structure, respectively, black indicates the ice sheet response to '3D ref'. Dashed lines show the response for East Antarctica (75% of the ice-covered area), dotted for West Antarctica (25%)~~, and (on the left) solid lines the sum of both~~. Olive lines show the reconstructions from ICE-6G_C. Melt water pulse 1A is indicated as 'MWP1a'.
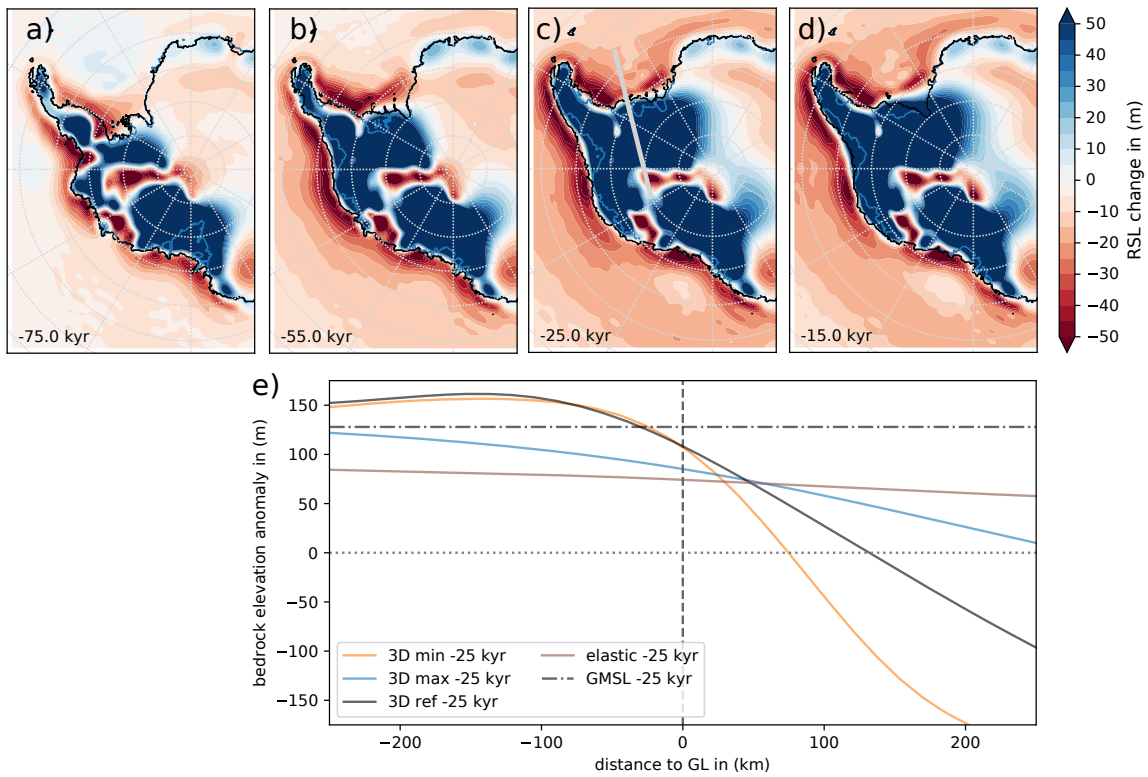
Figure S 5. Difference in RSL between '3D ref' and '3D max' in first iteration at four snapshots during last glaciation, showing peripheral forebulge (red shading) near advancing grounding lines in West Antarctica (black for '3D ref' and blue for '3D max'). Panel e) shows the bedrock elevation change (negative RSL change) along a transect through Ronne Ice Shelf (see grey line in c) with respect to initial bed topography in first iteration at 25 kyr BP, centered around the actual grounding line (GL) position (dashed). Subsidence in the grounded part to the right leads to uplift of a peripheral forebulge in front of the advancing GL (left), in particular for '3D min' case. Positive values indicate a water depth (RSL) lowering, which is a combination of viscoelastic, but also gravitational and rotational effects on top of the barystatic (mean) sea level change (dash-dotted). In the '3D max' case, no forebulge evolves within 250 km distance from the GL, similar to the purely elastic case (brown).
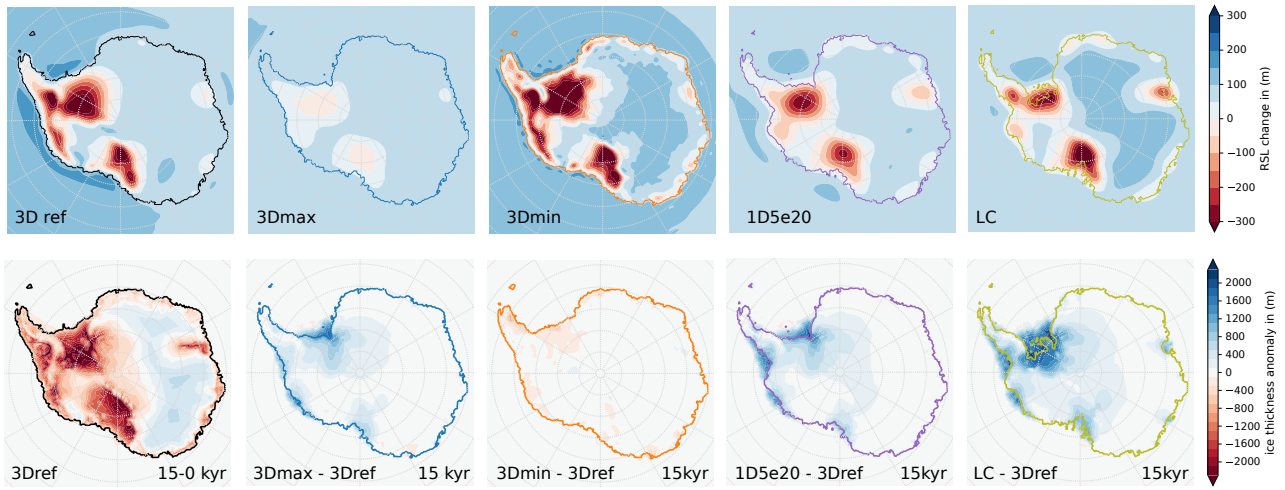
Figure S 6. RSL and ice thickness change since 15 kyr BP, in coupled simulations, for different 3D structures as in Sect. 3.2, and with respect to 1D Earth structure analogous to Lingle-Clark model (LC), as in Sect. 3.3. Corresponding grounding lines at LGM colored. In the lower row, ice thickness anomaly is between LGM (15 kyr BP) and present-day (0 kyr BP) for '3D ref' in the first panel. For the other panels anomaly is between LGM states of different Earth structures.

~~Global (logarithmic) lateral mean of 3D Earth structures a), Sea-level equivalent ice volume b) and ice flux over last 20 kyr c)~~
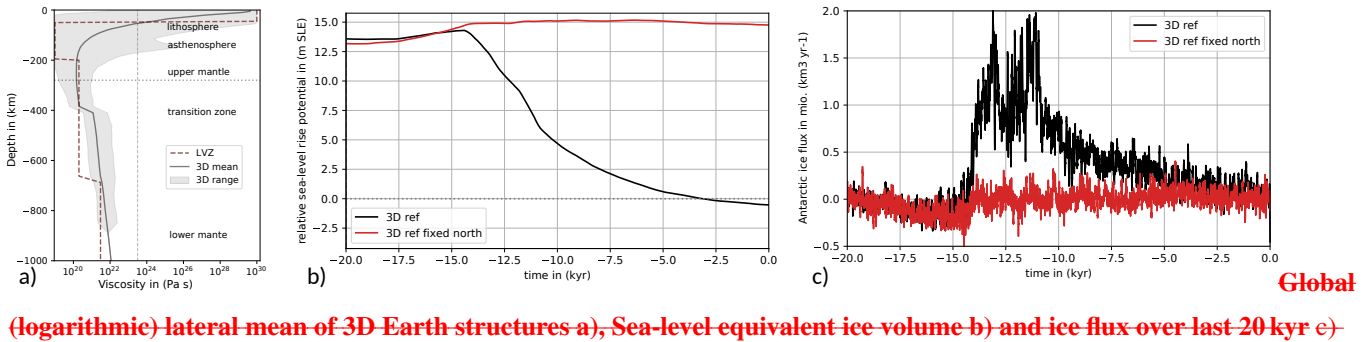
Figure S 7. Global (logarithmic) lateral mean of 3D Earth structures a), sea-level rise potential relative to preset day b) and ice flux over last 20 kyr c) in experiments with evolving (black) and fixed (red) northern hemisphere deglaciations, analogous to Fig. 2b and Fig. 3a in Gomez et al. (2020). Ice flux, as change in total Antarctic ice volume, has been smoothed with a 100-yr running mean ~~over 100~~. Red dotted line in a) shows 1D Earth structure ('LVZ') used by Gomez et al. (2020). Vertical line denotes threshold of $> 10^{23.5}$ Pa s defining the lithosphere thickness.
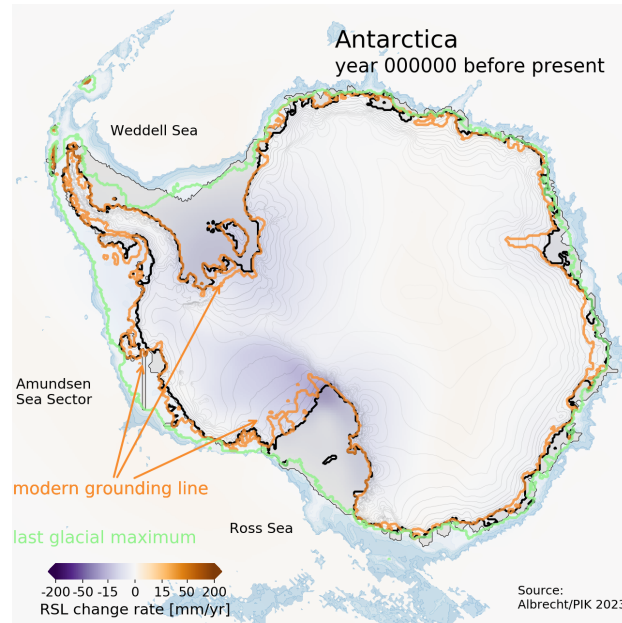
Video S 1: **Change rate of relative sea level (RSL) in Antarctica over the last 25 kyr from a coupled ice sheet–solid Earth model system with reference 3D Earth structure '3D ref'.** Black delineates the grounding line (GL), thin grey the calving front. Green is the GL extent at Last Glacial Maximum, orange the observed present-day GL. Inset shows the global mean sea level change with far-field change rates of up to $50\,\mathrm{mm\,yr^{-1}}$ at around $14.5\,\mathrm{kyr\,BP}$, the Meltwater Pulse 1A. Viscoelastic bedrock uplift in response to marine ice sheet retreat can cause near-field sea level drop of up to $-200\,\mathrm{mm\,yr^{-1}}$. Color scale is double logarithmic. Light grey contours indicate ice surface elevation, blue shading indicates the continental shelf up to $1800\,\mathrm{m}$ depth. See Video S 1 at: https://doi.org/10.5446/65479

Sensitivity of Antarctic Ice Sheet response to spatial variability in 3D Earth structures

20 After we have investigated the Antarctic Ice Sheet response coupled to VILMA for the reference 3D Earth structure '3D ref' (v_0.4_s16) compared to high and low viscosity end member 3D structures '3D min' and '3D max', we will now compare the ice sheet response to different 3D structure classes, obtained from the data compilation in Bagge et al. (2020) following their nomenclature. First, we test for another Class-I-type 3D structure '3D glob' (v_1.0_s16), with larger conversion factor (i.e., activation enthalpy factor) between temperature and viscosity and hence larger lateral variability (see range in Fig. S 10a),

25 but also with a higher global log-mean asthenosphere viscosity and a thicker lithosphere. For this Earth structure, VILMA-standalone simulations provide the best fit to a global dataset of present-day uplift rates (Bagge et al., 2023). We also consider the Class-II 3D structure '3D ant' (v_1.0_sc06) with the best fit to a subset of these dataset around Antarctica (36 stations) and with a similar lateral variability, but even higher viscosity in the upper mantle (below 210 km) and lower viscosity in the transition zone at the top of the upper mantle (below 410 km depth). For comparison, we apply the intermediate Class-III 3D

30 Earth structure '3D trans' (v_1.0_sc06b) with no strong viscosity jump between the upper mantle and the transition zone. All considered 3D Earth structure classes intersect at the top of the transition zone at a depth of 410 km, and converge in the lower mantle below the transition zone (below 670 km).

They can be distinguished by

- the viscosity in the upper mantle and transition zone, determined by the radial viscosity profile

35 - the lithosphere thickness, determined by the conversion factor and

- the lateral variablity, determined by the conversion factor.

~~In our coupled simulations, the range of deglacial response of the Antarctic Ice Sheet volume to variation in 3D Earth structure classes is comparably small, with largest differences of about 3 at LGM (Fig. S 10c) obtained for '3D ref', which also shows the largest sea-level relevant ice volume in Antarctica. Among the considered classes, '3D ref' has the lowest global~~

40 ~~mean upper-mantle viscosity, the thinnest lithosphere (Fig S 9) and the smallest global range (lateral variability, factor 0.4). For larger lateral variability (factor 1.0) we find for increasing upper mantle viscosity and decreasing lower mantle viscosity (s16, sc06b, sc06, see Fig. S 10a) slightly decreasing ice volumes at LGM. The trajectories of deglacial ice loss over the last 15 is similar in all classes, converging after 10 in the coupled simulations (Fig. S 10c). Already in the first iteration, the three classes with similar lateral variability and lithosphere thickness ('3D glob', '3D trans' and '3D ant') show a very similar ice volume~~

45 ~~response since LGM, while for '3D ref' the LGM ice volume is larger and the present-day ice volume is smaller (compare transparent lines in Fig. S 10c). Also, the convergence rate for the iterative optimization of present-day bed topography is lowest for '3D ref'. The present-day anomaly is alternating with each iteration and it takes 6 iterations instead of 3 to reach an RMSE below 10 (cf. Fig. 4 and Fig. S 10b). Likely, this effect is caused by the thin lithosphere, and is even more pronounced for the lower end '3D min' (Fig. 3c).~~
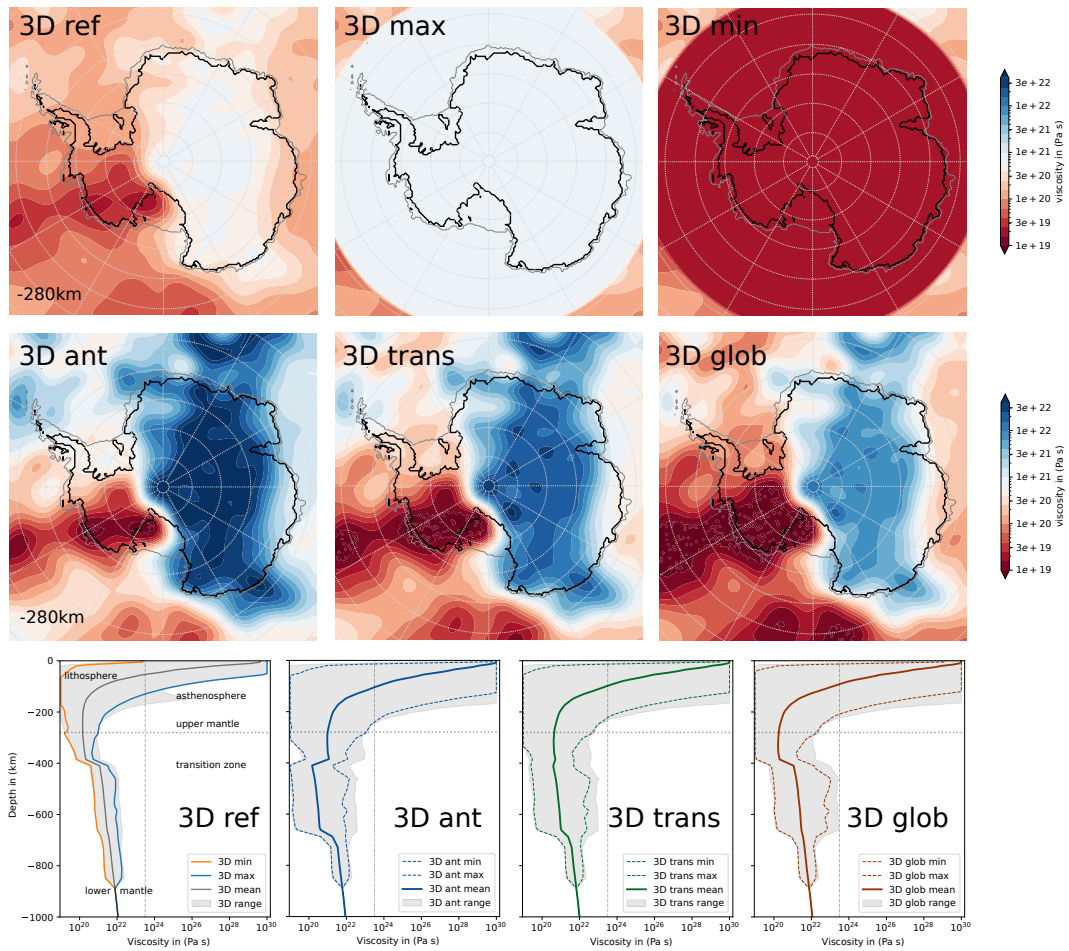
Figure S 8. Earth structures underneath Antarctica with upper-mantle viscosity shown at 280 km depth for the six different 3D structures considered. Vertical profiles show global range, logarithmic mean and minimum and maximum values in Antarctic domain for four of the 3D Earth structures. Note that colorbar range differs from that in Fig. 5b.
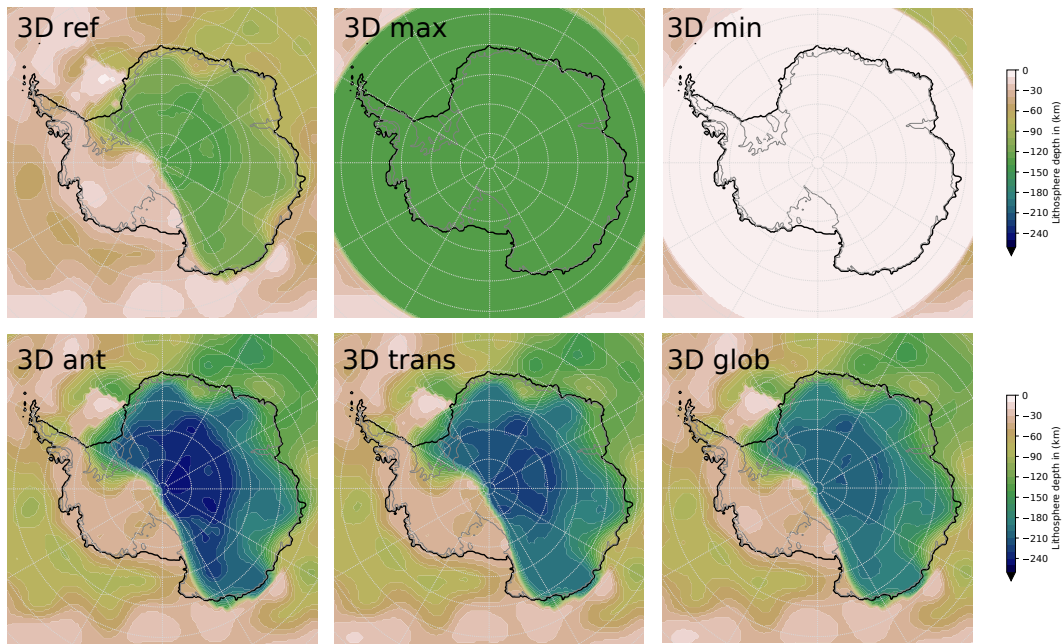
Figure S 9. Lithosphere thickness underneath Antarctica for the six different 3D structures considered. Note that colorbar range differs from Fig. 5c.

50   In our coupled simulations, the range of deglacial response of the Antarctic Ice Sheet ~~volume~~ SLRP to variation in 3D Earth structure classes is comparably small, with largest differences of about 3 m SLE at LGM (Fig. S 10c) obtained for '3D ref', which also shows the largest ~~sea-level relevant ice volume~~ SLRP in Antarctica. Among the considered classes, '3D ref' has the lowest global mean upper-mantle viscosity, the thinnest lithosphere (Fig S 9) and the smallest global range (lateral variability, factor 0.4). For larger lateral variability (factor 1.0) we find for increasing upper mantle viscosity and decreasing lower mantle

55   viscosity (s16, sc06b, sc06, see Fig. S 10a) slightly decreasing ~~ice volumes~~ SLRP at LGM. The trajectories of deglacial ice loss over the last 15 kyr is similar in all classes, converging after 10 kyr BP in the coupled simulations (Fig. S 10c). Already in the first iteration, the three classes with similar lateral variability and lithosphere thickness ('3D glob', '3D trans' and '3D ant') show a very similar ice volume (SLRP) response since LGM, while for '3D ref' the LGM ice volume is larger and the present-day ice volume is smaller (compare transparent lines in Fig. S 10c). Also, the convergence rate for the iterative optimization

60   of present-day bed topography is lowest for '3D ref'. The present-day anomaly is alternating with each iteration and it takes 6 iterations instead of 3 to reach an RMSE below 10 m (cf. Fig. 4 and Fig. S 10b). Likely, this effect is caused by the thin lithosphere, and is even more pronounced for the lower end '3D min' (Fig. 3c).
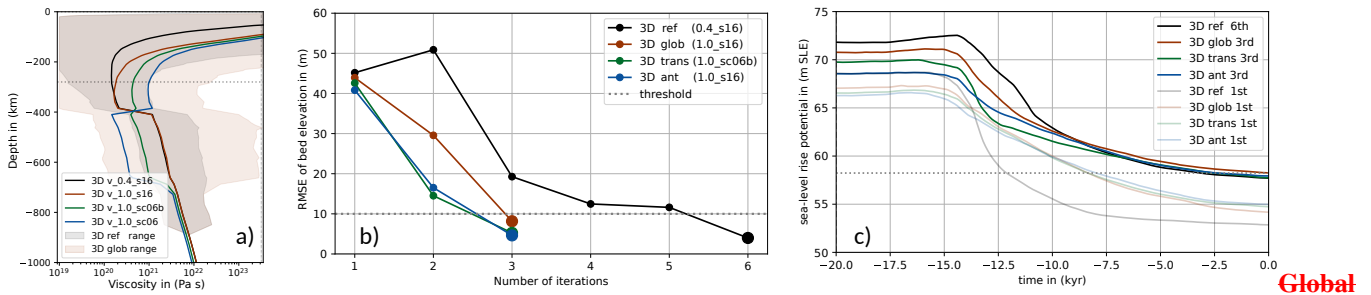
Figure S 10. Global (logarithmic) lateral mean viscosity of 3D Earth structures a), RSL convergence at present b) and corresponding SLRP from Antarctica c) over the last 20 kyr for different 3D Earth model configurations. Black color indicates the reference 3D Earth structure '3D ref' (v_0.4_s16, Class-I), red-brown a similar 3D structure but with more lateral variability '3D glob' (v_1.0_s16, Class-I), green an intermediate 3D structure '3D trans' (v_1.0_sc06b, Class-III) and dark-blue the 3D structure that has an opposite viscosity jump between the upper mantle and the transition zone '3D ant' (v_1.0_sc06, Class-II). In a) the range between global mininum and maximum viscosity for '3D ref' is shaded in grey, and redish for the '3D glob' Earth structure with larger lateral variability and thicker lithosphere. In c) for comparison, first iteration results are shown in transparent colors.

References

Adhikari, S., Ivins, E. R., Larour, E., Caron, L., and Seroussi, H.: A kinematic formalism for tracking ice–ocean mass exchange on the earth's surface and estimating sea-level change, The Cryosphere, 14, 2819–2833, https://doi.org/10.5194/tc-14-2819-2020, 2020.

Bagge, M., Klemann, V., Steinberger, B., Latinovic, M., and Thomas, M.: 3D Earth structures for glacial-isostatic adjustment models, V. 1.0, GFZ Data Services, https://doi.org/10.5880/GFZ.1.3.2020.004, 2020.

Bagge, M., Klemann, V., Steinberger, B., Latinović, M., and Thomas, M.: Glacial-Isostatic Adjustment Models Using Geodynamically Constrained 3D Earth Structures, Geochemistry, Geophysics, Geosystems, 22, e2021GC009 853, https://doi.org/10.1029/2021GC009853, 2021.

Bagge, M., Boergens, E., Balidakis, K., Klemann, V., and Dobslaw, H.: A validation method for modelled present-day GIA uplift rates against space geodetic data, Solid Earth (in prep.), 2023.

Fretwell, P., Pritchard, H. D., Vaughan, D. G., Bamber, J. L., Barrand, N. E., Bell, R., Bianchi, C., Bingham, R. G., Blankenship, D. D., Casassa, G., Catania, G., Callens, D., Conway, H., Cook, A. J., Corr, H. F. J., Damaske, D., Damm, V., Ferraccioli, F., Forsberg, R., Fujita, S., Gim, Y., Gogineni, P., Griggs, J. A., Hindmarsh, R. C. A., Holmlund, P., Holt, J. W., Jacobel, R. W., Jenkins, A., Jokat, W., Jordan, T., King, E. C., Kohler, J., Krabill, W., Riger-Kusk, M., Langley, K. A., Leitchenkov, G., Leuschen, C., Luyendyk, B. P., Matsuoka, K., Mouginot, J., Nitsche, F. O., Nogi, Y., Nost, O. A., Popov, S. V., Rignot, E., Rippin, D. M., Rivera, A., Roberts, J., Ross, N., Siegert, M. J., Smith, A. M., Steinhage, D., Studinger, M., Sun, B., Tinto, B. K., Welch, B. C., Wilson, D., Young, D. A., Xiangbin, C., and Zirizzotti, A.: Bedmap2: improved ice bed, surface and thickness datasets for Antarctica, The Cryosphere, 7, 375–393, https://doi.org/10.5194/tc-7-375-2013, 2013.

Goelzer, H., Coulon, V., Pattyn, F., De Boer, B., and Van De Wal, R.: Brief communication: On calculating the sea-level contribution in marine ice-sheet models, The Cryosphere, 14, 833–840, https://doi.org/10.5194/tc-14-833-2020, 2020.

Gomez, N., Weber, M. E., Clark, P. U., Mitrovica, J. X., and Han, H. K.: Antarctic ice dynamics amplified by Northern Hemisphere sea-level forcing, Nature, 587, 600–604, https://doi.org/10.1038/s41586-020-2916-2, 2020.